iScience

CellPress
OPEN ACCESS

Article

Quantitative proteomics and RNA-sequencing of mouse liver endothelial cells identify novel regulators of BMP6 by iron

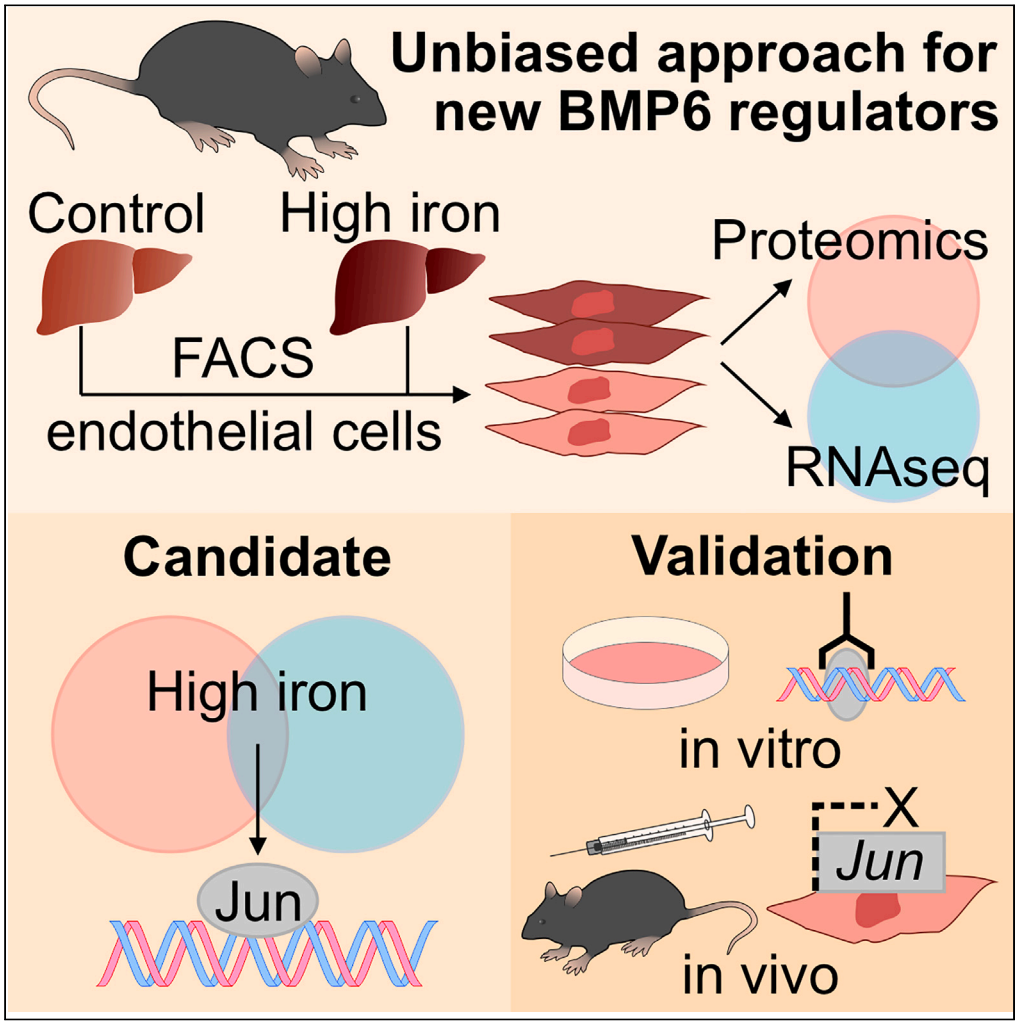

Allison L. Fisher, Chia-Yu Wang, Yang Xu, ..., Wojciech Fendler, Joseph D. Mancias, Jodie L. Babitt

Babitt.jodie@mgh.harvard.edu

Highlights

c-Jun pathway is activated by iron together with *Bmp6* in liver endothelial cells

c-Jun binds to *Bmp6* gene regulatory regions in an iron-dependent fashion

Jun inhibition blunts *Bmp6* induction by iron in liver endothelial cells and mice

Conditional KO mice suggest c-Jun is genetically redundant or has multiple actions

Fisher et al., iScience *26*, 108555
December 15, 2023
https://doi.org/10.1016/j.isci.2023.108555

iScience

CellPress
OPEN ACCESS

Article

Quantitative proteomics and RNA-sequencing of mouse liver endothelial cells identify novel regulators of BMP6 by iron

Allison L. Fisher,[1,6] Chia-Yu Wang,[1,6] Yang Xu,[1] Sydney Phillips,[1] Joao A. Paulo,[2] Beata Małachowska,[3,4] Xia Xiao,[1] Wojciech Fendler,[3,5] Joseph D. Mancias,[5] and Jodie L. Babitt[1,7,*]

SUMMARY

Hepcidin is the master hormone governing systemic iron homeostasis. Iron regulates hepcidin by activating bone morphogenetic protein (BMP)6 expression in liver endothelial cells (LECs), but the mechanisms are incompletely understood. To address this, we performed proteomics and RNA-sequencing on LECs from iron-adequate and iron-loaded mice. Gene set enrichment analysis identified transcription factors activated by high iron, including Nrf-2, which was previously reported to contribute to BMP6 regulation, and c-Jun. *Jun* (encoding c-Jun) knockdown blocked *Bmp6* but not Nrf-2 pathway induction by iron in LEC cultures. Chromatin immunoprecipitation of mouse livers showed iron-dependent c-Jun binding to predicted sites in *Bmp6* regulatory regions. Finally, c-Jun inhibitor blunted induction of *Bmp6* and hepcidin, but not Nrf-2 activity, in iron-loaded mice. However, *Bmp6* and iron parameters were unchanged in endothelial *Jun* knockout mice. Our data suggest that c-Jun participates in iron-mediated BMP6 regulation independent of Nrf-2, though the mechanisms may be redundant and/or multifactorial.

INTRODUCTION

Iron is essential for cellular and metabolic processes but is toxic in excess. The liver hormone hepcidin regulates systemic iron homeostasis by binding to its receptor ferroportin to induce its degradation and inhibit iron export.[1] This results in iron retention in iron-absorptive intestinal cells and iron-recycling macrophages, thereby lowering plasma iron levels. In pregnancy or iron deficiency where more iron is needed for erythropoiesis, hepcidin is suppressed to increase iron bioavailability.[2,3] On the other hand, iron loading and inflammation induce hepcidin to prevent iron overload and restrict iron availability to infectious organisms.[2,4,5] Pathological dysregulation of hepcidin causes iron disorders, including hereditary hemochromatosis, β-thalassemia, iron-refractory iron deficiency anemia, and anemia of chronic disease.[6,7]

Iron and most other regulatory signals modulate hepcidin through the bone morphogenetic protein (BMP) 6-SMAD pathway.[6,7] BMPs are a subset of the transforming growth factor β (TGF-β) superfamily of signaling molecules that are involved in an array of organismal processes including embryonic development, cellular survival, and differentiation. In addition to these processes, BMP6 and BMP2 are involved in regulation of systemic iron homeostasis via SMAD signaling proteins. Mechanistically, high iron induces the production of BMP6 and, to a lesser extent, BMP2 from endothelial cells in the liver.[8–10] BMP6 and BMP2 bind to the BMP receptor complex on the hepatocyte membrane to initiate the phosphorylation of SMAD1/5/8 transcription factors.[6,7] Phosphorylated SMAD1/5/8 complexes with SMAD4 and translocates to the nucleus, binding to the hepcidin promoter to upregulate transcription.[6,7] Mice deficient in either endothelial *Bmp6* or *Bmp2* develop hepcidin deficiency and iron overload, demonstrating that endothelial cells are the source of BMP production for hepcidin regulation.[9,10] Although these genetic mouse models do not exclude the contribution of endothelial cells in other organs, iron-mediated induction of BMP6 and BMP2 only occurs in the liver.[8,9,11–13] BMP6 and BMP2 function together in hepcidin regulation, possibly as heterodimers, since ablating endothelial *Bmp6* does not further suppress hepcidin in endothelial *Bmp2* knockout mice and vice versa.[14] Moreover, BMP6 is considered to be the rate limiting ligand in activation of this signaling pathway since BMP6 is expressed to a lesser degree than BMP2 under basal conditions yet is more responsive to iron.[8]

The underlying cellular mechanisms by which iron induces BMP6 production in liver endothelial cells are incompletely understood. In physiologic conditions, transferrin-bound iron is the predominant iron species in circulation. However, in liver endothelial cells, this form of iron was shown to only have a minor role in regulating BMP6 expression and iron homeostasis.[15,16] When iron levels increase and the transferrin-binding

[1]Nephrology Division and Endocrine Unit, Massachusetts General Hospital, Harvard Medical School, Boston, MA, USA
[2]Department of Cell Biology, Harvard Medical School, Boston, MA, USA
[3]Department of Biostatistics and Translational Medicine, Medical University of Lodz, Lodz, Poland
[4]Department of Radiation Oncology, Albert Einstein College of Medicine, NYC, NY, USA
[5]Department of Radiation Oncology, Dana-Farber Cancer Institute, Boston, MA, USA
[6]These authors contributed equally
[7]Lead contact
*Correspondence: Babitt.jodie@mgh.harvard.edu
https://doi.org/10.1016/j.isci.2023.108555

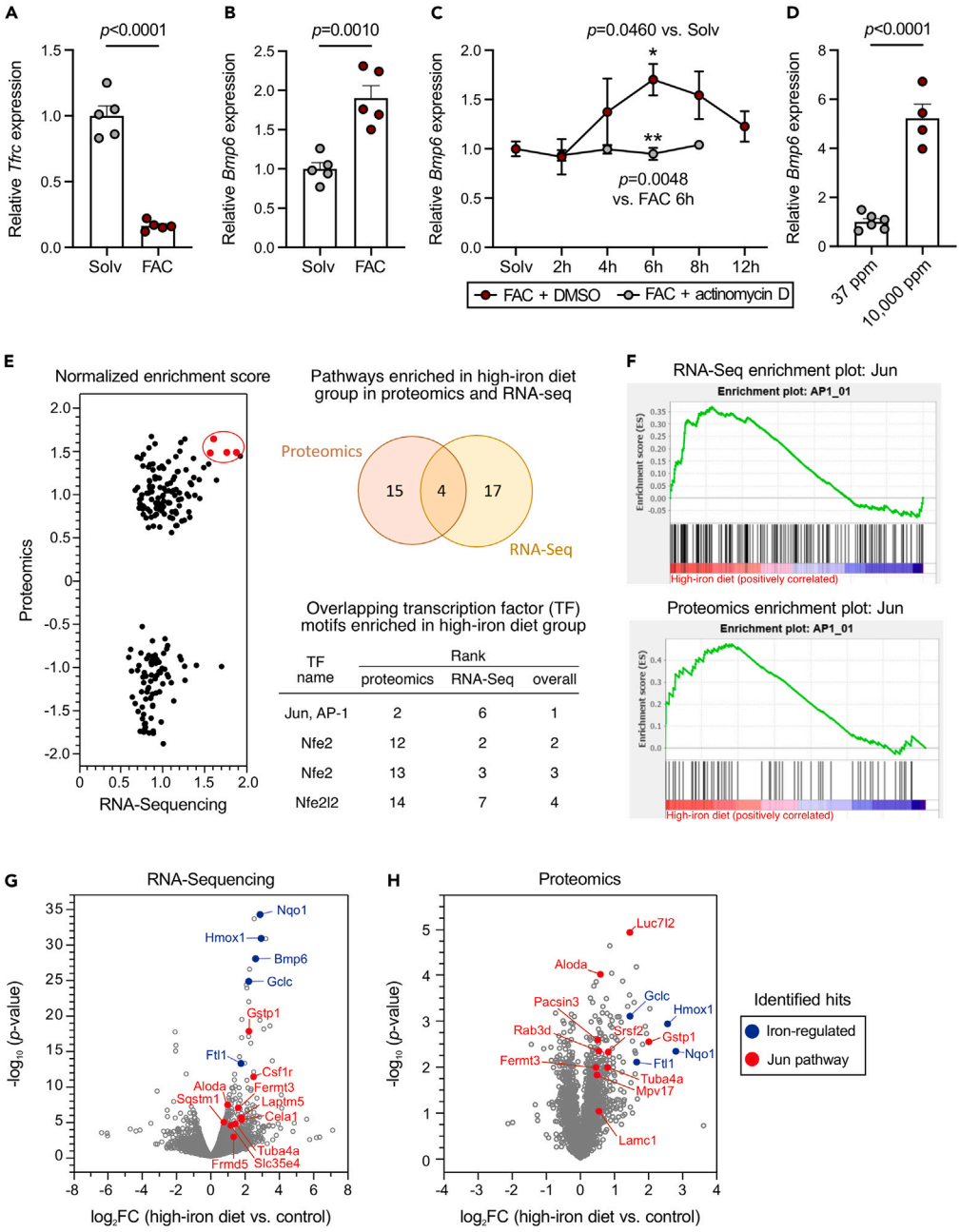

Figure 1. RNA-sequencing and proteomics identify Jun as a top ranked transcription factor activated by iron in liver endothelial cells

(A-B) Primary liver endothelial cells were treated with 200 μg/mL ferric ammonium citrate (FAC, n = 5) or PBS (Solv, n = 5) for 6 h and analyzed for (A) *Tfrc* and (B) *Bmp6* expression relative to *Rpl19* by qRT-PCR.

(C) Time course of *Bmp6* expression relative to *Rpl19* in primary liver endothelial cells treated with Solv (n = 4) or 200 μg/mL FAC in the absence or presence of 2 μg/mL actinomycin D for 2–12 h (n = 4/group).

(D–G) Three-week-old wildtype 129S6/SvEvTac male mice were fed a purified diet with 37 ppm ferric citrate or 10,000 ppm carbonyl iron for 4 weeks (*n* = 4–6/diet). Liver endothelial cells were isolated by FACS and analyzed for (D) *Bmp6* expression relative to *Rpl19* by qRT-PCR to confirm *Bmp6* induction by iron *in vivo*.

(E–H) Liver endothelial cells from 3 to 4 mice/group were subjected to RNA-sequencing and quantitative proteomics analyses, and datasets were analyzed by gene set enrichment analysis (GSEA) looking for proteins/transcripts associated with a given transcription factor pathway within the ranked list and calculating an enrichment score depending on the set being up or downregulated. (E) Plotting normalized enrichment score identified four overlapping motifs enriched in the high-iron group. (F) Enrichment plots show the enrichment score (ES) values on the Y axis representing the strength of association of pathway components with the high-iron diet group. The bars below the figure represent the relative position of genes/proteins regulated by Jun/AP-1 in the list of all genes/proteins ranked from the most positively associated (red) to the ones with a negative association (blue). Expanded enrichment plots are provided in Figure S2. (G–H) Volcano plots illustrate (G) mRNA and (H) protein abundance differences in liver endothelial cells isolated from mice fed high-iron versus iron-sufficient (control) diets. Volcano

Figure 1. *Continued*

plots display the –log10(p value) versus the log2 of the relative mRNA/protein abundance of mean high-iron to control. Red circles represent genes/proteins in the Jun/AP-1 pathway and blue circles represent genes/proteins that are known to be regulated by iron. The remainder of genes/proteins are represented as gray circles. Bar and line graphs represent mean ± SEM with bar graphs showing individual points that indicate the number of independent experiments or animals. (A–D) Statistical differences between groups were determined by two-tailed Student's *t* test for normally distributed values or (C) one-way analysis of variance with Holm-Sidak method of multiple comparisons (FAC 6h versus Solv). *p = 0.0406 vs Solv control; **p = 0.0048 vs FAC + DMSO at 6 h. See also Figures S1 and S2.

capacity is exceeded, non-transferrin bound iron (NTBI) appears. NTBI is toxic, and its accumulation within cells and tissues ultimately leads to dysfunction. Like hepatocytes,[17] liver endothelial cells take up NTBI at a faster rate than transferrin-bound iron.[15] How NTBI is taken up by liver endothelial cells is unknown, but many uptake pathways have been proposed.[15,18] By generating reactive oxygen species in mitochondria, NTBI activates the antioxidant response transcription factor nuclear factor-erythroid derived 2 like 2 (Nfe2l2, also known as Nrf-2), which induces *Bmp6* in liver endothelial cell cultures and mice.[19] However, iron overload retains some ability to induce *Bmp6* and hepcidin in global *Nfe2l2* (encoding Nrf-2) knockout mice,[19] suggesting that additional Nrf-2-independent regulatory mechanisms exist.

In this study, we used RNA-sequencing and mass spectrometry-based quantitative proteomics to identify candidate regulators of BMP6 by iron in liver endothelial cells. We focused on BMP6 as the rate limiting ligand. We utilized primary liver endothelial cell cultures, publicly available endothelial cell sequencing data from ENCODE,[20,21] and mouse models to validate the candidate regulators in multiple systems.

RESULTS

RNA-sequencing and proteomics identify Jun as a top ranked transcription factor activated by iron in liver endothelial cells

We previously reported that iron induces *Bmp6* mRNA expression in a cell autonomous fashion in a primary mouse liver endothelial cell culture system.[15,19] To investigate the mechanisms, we tested whether iron-mediated regulation of *Bmp6* expression occurs at the transcriptional level. As previously reported,[15,19] treatment of primary liver endothelial cells with ferric ammonium citrate (FAC), a common form of NTBI in iron-overloaded patient plasma,[22,23] efficiently loaded cells with iron and did not induce apoptosis, as reflected by suppressed expression of transferrin receptor 1 (*Tfrc*) mRNA (Figure 1A), presence of ferric iron by Perl's iron stain, and lack of TUNEL stain (Figure S1). FAC treatment also significantly induced *Bmp6* expression (Figure 1B), confirming cell autonomous regulation of *Bmp6* by iron. Incubation with the transcriptional inhibitor actinomycin D completely blocked the induction of *Bmp6* by FAC treatment (Figure 1C), demonstrating that iron regulates *Bmp6* via a transcriptional mechanism. We were unable to determine if iron also impacts translational regulation of BMP6 due to the lack of commercial antibodies that reliably detect the endogenous BMP6 protein by Western blotting.[11]

To investigate upstream regulator(s) that control *Bmp6* regulation by iron, we performed unbiased RNA-sequencing and mass spectrometry-based quantitative proteomics on liver endothelial cells isolated from mice fed a matched, purified iron-sufficient diet (37 ppm iron) or high-iron diet (10,000 ppm iron) for 4 weeks. Liver endothelial cells were isolated from whole livers by fluorescence-activated cell sorting (FACS) to yield a highly enriched endothelial cell population.[9,19] As expected, liver endothelial cells isolated from mice fed the high-iron diet exhibited significantly higher *Bmp6* expression compared to mice fed the iron-sufficient diet (Figure 1D), confirming iron-mediated *Bmp6* regulation. Isolated liver endothelial cells underwent RNA-sequencing and proteomics, and results from both datasets were subjected to gene set enrichment analysis (GSEA) to identify groups of proteins/transcripts associated with a given transcription factor pathway that were differentially expressed between the two iron diet groups (Figure 1E). Gene sets were overlaid in search of overlapping results from both datasets to identify higher confidence targets. Enrichment map visualization identified pathways that were upregulated and downregulated by iron in both datasets (Figure S2A). Pathways that were upregulated in the high-iron diet group included iron uptake and transport, oxidative stress response, and mitochondrial function, among others (Figure S2A). Pathways that were downregulated in the high-iron diet group (upregulated in control group) included immune response, cell cycle regulation, and mRNA processing and metabolism (Figure S2A).

Importantly, GSEA identified overlapping protein/transcript sets that were enriched by the high-iron diet with sequences recognized by three transcription factors in both datasets (Figure 1E). The top-ranked transcription factors included c-Jun protooncogene, AP-1 transcription factor subunit (c-Jun, encoded by *Jun*), and nuclear factor, erythroid derived 2 (Nfe2), and Nrf-2 (Figure 1E). These transcription factors are known to be activated by oxidative stress as part of the antioxidant response.[24–28] Notably, Nrf-2 was demonstrated to have a functional role in *Bmp6* regulation under high iron conditions,[19] providing validation of this approach. We focused subsequent efforts on the potential role of c-Jun as the top-ranked transcription factor pathway identified by this analysis.

Enrichment plots for c-Jun depict a positive correlation between c-Jun target transcripts and the high-iron diet group in the RNA-Seq and proteomics datasets, demonstrating consistency in the two methods (Figures 1F, S2B, and S2C). Furthermore, volcano plots of both datasets highlight the differential upregulation of transcripts/proteins in the c-Jun transcription factor pathway by the high-iron diet (Figures 1G and 1H, red dots). Volcano plots also demonstrated upregulation of *Bmp6* itself and other transcripts/proteins known to be induced by iron, including ferritin light chain (*Ftl1*) and Nrf-2 targets *Gclc, Hmox1,* and *Nqo1* (Figures 1G and 1H, blue dots). Taken together, our data suggest that in addition to Nrf-2, c-Jun may also contribute to *Bmp6* transcriptional regulation in response to iron.

Validation of c-Jun as a regulator of iron-mediated Bmp6 expression in liver endothelial cells

To validate c-Jun as a candidate regulator of *Bmp6* expression by high iron, we utilized the primary liver endothelial cell culture model. Cells were analyzed for the impact of siRNA knockdown of endogenous *Jun* compared to cells treated with control siRNA for FAC-mediated

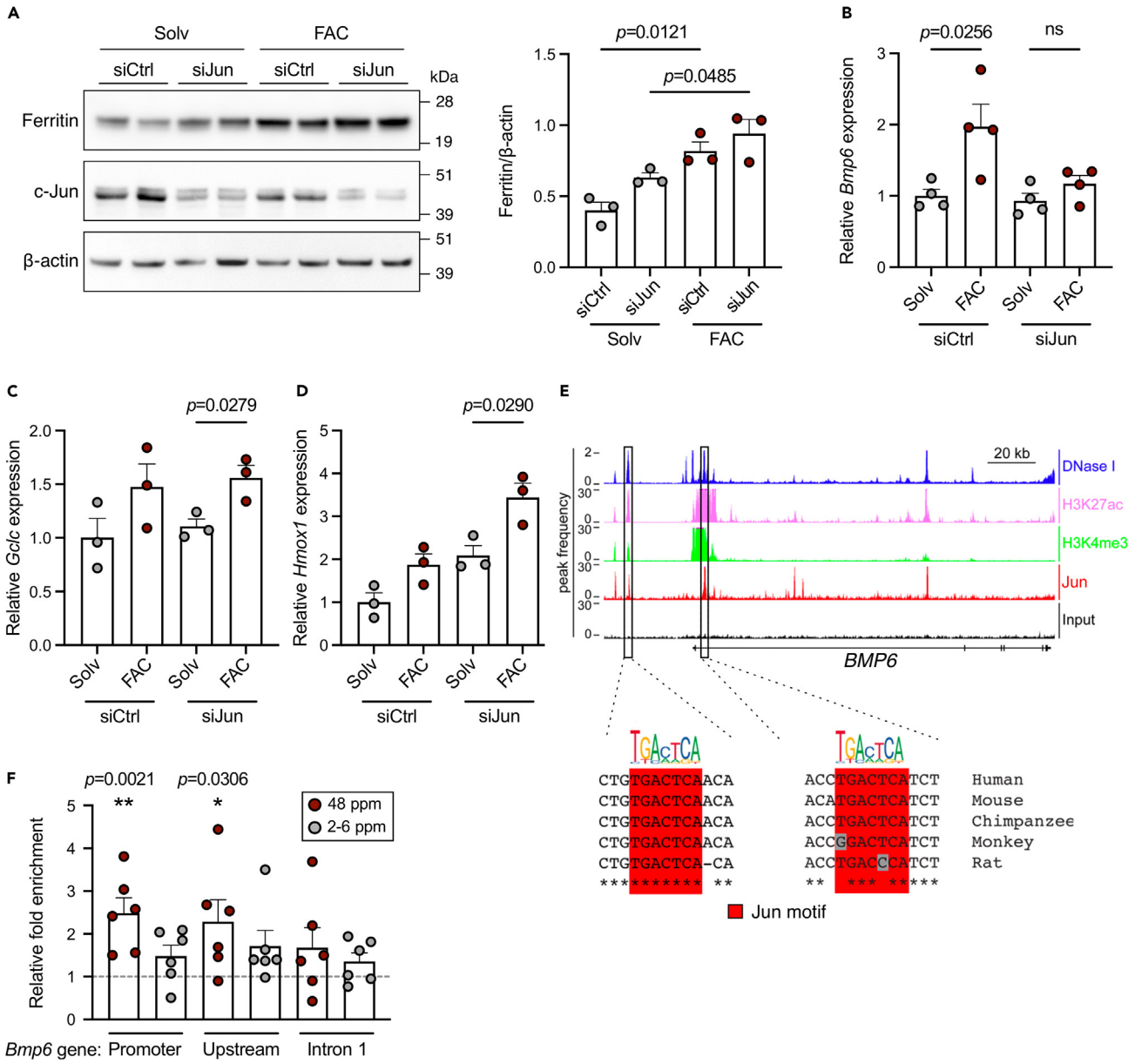

Figure 2. Validation of c-Jun as a regulator of iron-mediated *Bmp6* expression in liver endothelial cells

(A–D) Primary liver endothelial cells were treated with 40 nM control siRNA or siRNA targeting *Jun* for 48 h prior to treatment with 200 μg/mL ferric ammonium citrate (FAC) or PBS (Solv) for 6 h (n = 3–4/group). Cells were analyzed for (A) ferritin and total c-Jun protein relative to β-actin expression by Western blot and quantitation, and for (B) *Bmp6*, (C) *Gclc*, and (D) *Hmox1* relative to *Rpl19* mRNA expression by qRT-PCR.

(E) Chromatin immunoprecipitation (ChIP)-sequencing data for the human *BMP6* locus in umbilical vein endothelial cells. ChIP-seq data was downloaded from ENCODE. Black boxes depict peaks for Jun with corresponding consensus sequence motif TGACTCA indicated in red.

(F) Four-week-old wildtype C57BL/6J mice were fed a purified iron-deficient (2–6 ppm iron) or iron-sufficient (48 ppm iron) diet for 3 weeks (n = 6/group). Whole livers were subjected to ChIP using anti-c-Jun antibody and analyzed by qRT-PCR to measure binding of c-Jun to the promotor, upstream regulatory region, and intron 1 of the *Bmp6* gene, expressed relative to the IgG control antibody (dotted line). Primers were designed based on available ENCODE data from panel (E). Bar graphs represent mean ± SEM with individual points indicating the number of independent experiments or animals. Statistical differences between groups were determined by two-tailed Student's t test for normally distributed values or (B) one-way analysis of variance with Holm-Sidak method of multiple comparisons. *p = 0.0306 vs IgG control; **p = 0.0021 vs IgG control; ns, not significant. See also Figures S3, S4, and S7.

induction of *Bmp6* expression. Effective *Jun* knockdown was confirmed by over 70% reduction in *Jun* expression (Figure S3) and a reduction in total c-Jun protein (Figure 2A). *Jun* knockdown did not impact the ability of FAC to load cells with iron, as reflected by increases in ferritin protein in both groups (Figure 2A). Total c-Jun protein expression was not induced by FAC (Figure 2A), but we were unable to validate

commercially available phospho-c-Jun antibodies to test the activation of c-Jun directly in this model. As expected, *Bmp6* expression was induced by FAC within 6 h in cells treated with control siRNA (Figure 2B). Importantly, *Jun* knockdown blocked induction of *Bmp6* by FAC (Figure 2B), similar to what occurs with *Nfe2l2* (encoding Nrf-2) knockdown (Figure S4). Lack of an induction of *Bmp6* by FAC in *Jun* knockdown cells was not secondary to inhibition of Nrf-2 pathway activity, as *Jun* knockdown did not inhibit baseline or FAC-mediated induction of Nrf-2-target genes *Gclc* and *Hmox1* (Figures 2C and 2D). Together, these data suggest a direct functional role for c-Jun in regulating *Bmp6* in response to high iron in liver endothelial cells.

Using publicly available ENCODE data in human umbilical vein endothelial cells,[21] we identified two c-Jun consensus binding motifs (TGACTCA) within predicted *BMP6* regulatory regions, which are conserved among species (Figure 2E). Furthermore, ChIP-Seq data showed peaks for c-Jun binding in the location of both predicted binding sites (Figure 2E), suggesting a direct interaction between c-Jun and these *BMP6* regulatory regions. To validate these interactions in the liver *in vivo* and test whether these interactions are iron-responsive, whole livers from mice fed iron-deficient (2–6 ppm iron) or iron-sufficient (48 ppm iron) diets were subjected to ChIP-qPCR using c-Jun antibody and primers based on the ENCODE data to detect predicted c-Jun binding motifs in the upstream regulatory region and intron 1 of murine *Bmp6*. We also investigated iron-dependent interaction of c-Jun with the *Bmp6* promoter, although there was no c-Jun consensus binding motif identified in the promoter. We found a significant increase in c-Jun binding to the *Bmp6* promotor and the c-Jun binding motif in the upstream regulatory region of *Bmp6* in iron-sufficient livers, compared to IgG control, but not in iron-deficient livers (Figure 2F). However, no increase in c-Jun binding to the c-Jun binding motif in intron 1 of *Bmp6* was detected. Taken together, these data demonstrate that c-Jun binds to *Bmp6* regulatory regions in an iron-dependent fashion.

A small molecule inhibitor of c-jun phosphorylation blunts Bmp6 induction by an iron-loaded diet in mice

Next, we investigated the functional contribution of c-Jun to iron-mediated *Bmp6* regulation *in vivo*. We tested the impact of the broad-spectrum c-Jun N-terminal kinase (JNK) inhibitor SP600125, which blocks c-Jun phosphorylation,[29] on liver *Bmp6* mRNA expression and iron homeostasis parameters in mice maintained on an iron-sufficient diet (48 ppm iron) or switched to an iron-loaded diet (20,000 ppm iron) for 5 days. The iron-loaded diet significantly increased liver iron concentration but caused only a trend toward increased serum iron levels, irrespective of SP600125 treatment (Figures 3A and 3B). Despite a similar degree of iron loading, treatment with SP600125 blunted the induction of liver *Bmp6* as well as *Bmp2* expression by dietary iron (Figures 3C and 3D). Treatment with SP600125 also lowered liver hepcidin (*Hamp*) expression in the iron-loaded diet group (Figure 3E). *Hamp* expression was also reduced by SP600125 treatment in mice maintained on the iron sufficient diet (Figure 3E). Taken together, these data suggest that c-Jun has a functional role in regulating iron-mediated BMP ligand and hepcidin induction *in vivo*.

Interestingly, despite a previous study implicating a functional role of Nrf-2 in *Bmp6* and *Hamp* regulation by iron, the reductions in *Bmp6*, *Bmp2*, and *Hamp* by SP600125 occurred despite increases in Nrf-2 target transcripts *Gclc* and *Nqo1*, which were further potentiated by iron loading (Figures 3F and 3G). There was a similar tendency for *Jun* knockdown to induce the Nrf-2 target *Hmox1* and potentiate its iron-mediated induction in primary liver endothelial cell cultures (Figure 2D), although liver *Hmox1* was not significantly impacted by SP600125 or the iron-loaded diet in mice (Figure 3H). These data support the notion that Nrf-2 is not the sole mediator of *Bmp6* regulation by iron and that the *Bmp6*-, *Bmp2*-, and *Hamp*-inhibiting effects of SP600125 were not an indirect effect of inhibiting Nrf-2 activity.

Endothelial Jun knockout mice do not exhibit changes in liver Bmp6 expression or other iron homeostasis parameters

A limitation of the c-Jun inhibitor study is that the inhibitor acts globally, limiting the ability to ascertain the role of c-Jun in iron-mediated *Bmp6* regulation specifically in endothelial cells. To address this, we generated mice lacking *Jun* in endothelial cells using the *Stabilin2-Cre* driver (*Jun*$^{fl/fl}$*;Stab2-Cre+*) and littermate *Jun*$^{fl/fl}$*;Stab2-Cre*-controls.[30,31] We validated the conditional *Jun* knockout animals by isolating liver endothelial cells and macrophages (Kupffer cells) by magnetic sorting. We confirmed enrichment of liver endothelial cells by increased expression of the endothelial marker *Cd146*, and Kupffer cells by increased *Cd45* expression (Figures 4A and 4B). Importantly, we found ~80% reduction in *Jun* expression in liver endothelial cells, but comparable levels of *Jun* expression in Kupffer cells, from *Jun*$^{fl/fl}$*;Stab2-Cre+* mice compared with *Cre-* controls (Figures 4C and 4D). This aligns with our prior analysis of *Stabilin2-Cre* activity.[15] These results confirm that *Jun* knockdown is primarily restricted to endothelial cells in the liver and the contribution of macrophage *Jun* deletion, if any, is negligible.

We analyzed *Jun*$^{fl/fl}$*;Stab2-Cre+* and littermate *Jun*$^{fl/fl}$*;Stab2-Cre-* male and female mice after feeding either a purified iron-sufficient diet (48 ppm iron) or high-iron diet (10,000 p.m. iron) for 2 weeks starting at 6 weeks of age. As expected, liver iron, serum iron, transferrin saturation, liver *Bmp6* and *Hamp* expression were increased in iron-loaded mice compared to iron-sufficient mice of both genotypes (Figures 4E–4H and S5). However, we did not find any differences between sex- and diet-matched genotypes in liver or serum iron concentration, serum transferrin saturation, or whole liver expression of *Bmp6*, *Bmp2*, or *Hamp* (Figures 4E–4H and S5). A lack of impact on *Bmp6* expression was also confirmed in isolated liver endothelial cells (Figure S5). We also did not detect any changes in hemoglobin, hematocrit, or red blood cell indices between sex-and diet-matched genotypes with the exception of slightly increased mean corpuscular hemoglobin in *Jun*$^{fl/fl}$*;Stab2-Cre+* females on a high-iron diet (Tables S1 and S2). Together, these data suggest that the functional role of endothelial c-Jun in iron-mediated *Bmp6* regulation *in vivo* is redundant and/or requires coordinated activity in additional cell types beyond endothelial cells.

Since the c-Jun inhibitor study showed that SP600125 blunted *Bmp6* induction by iron despite potentiating the induction of Nrf-2 pathway targets (Figures 3C, 3F, and 3G), we considered the possibility that Nrf-2-mediated *Bmp6* induction may require c-Jun. We therefore tested whether the Nrf-2 activator CDDO-Im retained its ability to induce *Bmp6*[19] in *Jun* knockdown primary liver endothelial cell cultures and endothelial *Jun* knockout mice. As previously reported,[19] CDDO-Im treatment increased *Bmp6* mRNA expression in parallel with Nrf-2 targets *Gclc*

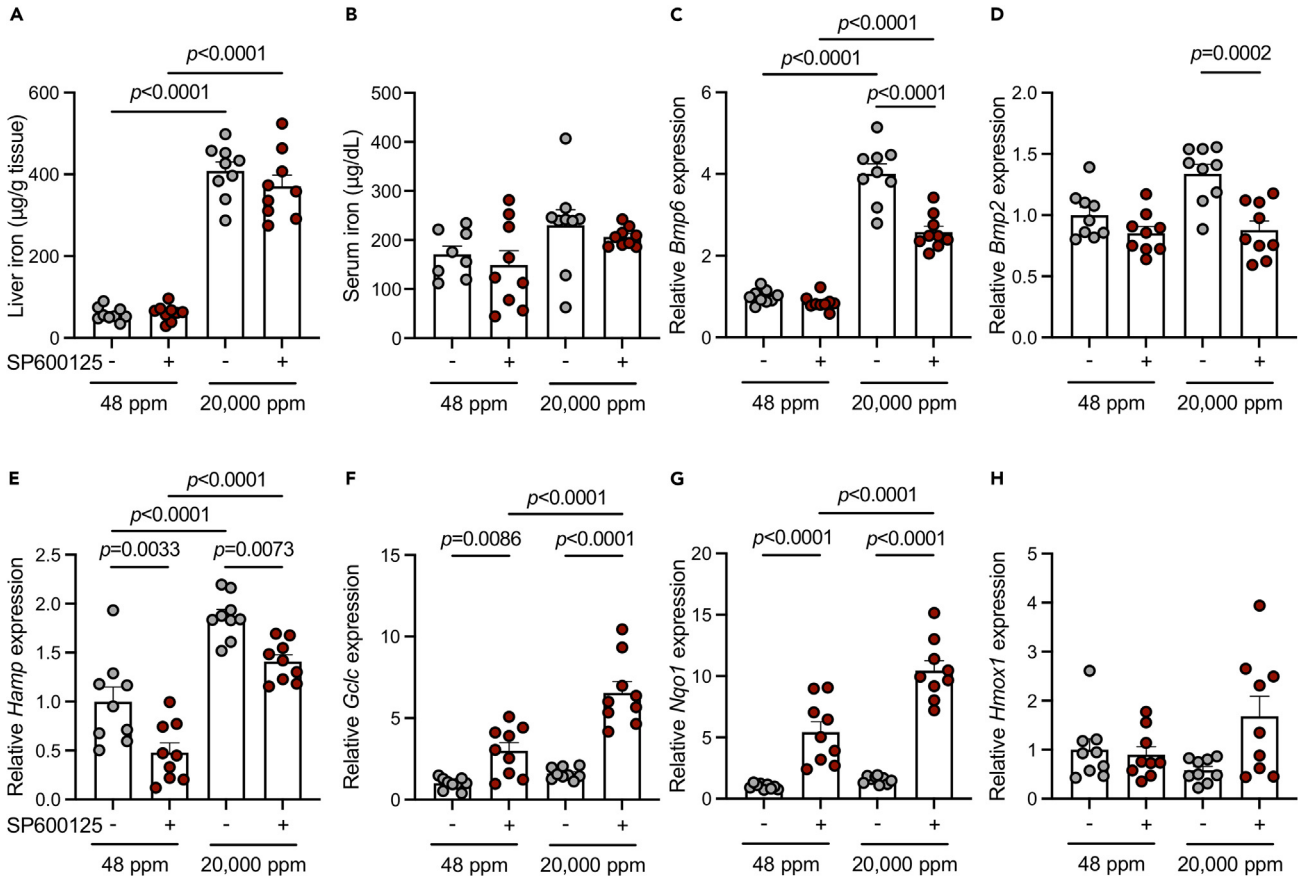

Figure 3. A small molecule inhibitor of c-Jun phosphorylation blunts *Bmp6* induction by an iron-loaded diet in mice

Four-week-old wildtype C57BL/6NTac female mice were fed purified iron-sufficient diet (48 ppm iron) for 3 days. On day 4, half of the mice were switched to high-iron diet (20,000 ppm iron) for the remainder of the experiment, while the remaining mice continued the iron-sufficient diet. Starting on day 3, mice in both groups received daily intraperitoneal injections of broad-spectrum JNK inhibitor SP600125 (2 mg/mouse), which blocks c-Jun phosphorylation, or DMSO for 5 days and were harvested 6 h after the final injection (n = 9/diet/treatment). Mice were analyzed for (A) liver iron concentration, (B) serum iron concentration, and hepatic expression of (C) *Bmp6*, (D) *Bmp2*, (E) *Hamp*, (F) *Gclc*, (G) *Nqo1*, and (H) *Hmox1* relative to *Rpl19* by qRT-PCR. Bar graphs represent mean ± SEM with individual points indicating the number of animals. Statistical differences between groups were determined by one-way analysis of variance with Holm-Sidak method of multiple comparisons.

and *Hmox1* in cells transfected with control siRNA (Figures S6A–S6C) However, *Jun* knockdown did not interfere with the induction of *Bmp6* or Nrf-2 targets by CDDO-Im (Figures S6A–S6C). Likewise, we found that CDDO-Im treatment similarly induced liver Nrf-2 activity and *Bmp6* expression in endothelial *Jun* knockout mice and *Cre-* controls (Figures S6D–S6F). Together these findings indicate that Nrf-2-mediated *Bmp6* induction does not require c-Jun.

DISCUSSION

Induction of liver endothelial cell *Bmp6* expression by iron is central to the adequate sensing of iron levels to control systemic iron homeostasis. Global or endothelial knockout or mutations of *Bmp6* results in iron overload in mice and humans,[32–35] and treatment with exogenous BMP6 ameliorates hemochromatosis in mice.[36] Although BMP6 is critical for the regulation of iron homeostasis and a therapeutic target to treat iron disorders, how iron regulates *Bmp6* expression is incompletely understood. The Nrf-2 pathway was previously shown to induce *Bmp6* expression as a cellular response to iron-mediated mitochondrial oxidative stress.[19] However, the residual induction of *Bmp6* expression by iron in global *Nfe2l2* knockout mice[19] suggests the existence of additional regulatory pathways.

Using unbiased RNA-sequencing and quantitative proteomics methodology coupled with GSEA, we identified c-Jun as a candidate transcription factor whose activity is induced by high-iron in liver endothelial cells concordantly with *Bmp6* expression. The Nrf-2 pathway was also one of the top hits, providing validation of this approach. In support of this finding, a review of the supplementary information published in a recent independent study of *Bmp6* regulation by iron using single-cell RNA-sequencing of mouse livers also demonstrated significant increases in c-Jun transcription factor pathway activity specifically in the liver sinusoidal endothelial cell populations in response to two different high iron conditions.[16] The prior study[16] differed from ours in the use of single-cell RNA-sequencing of whole liver rather than bulk

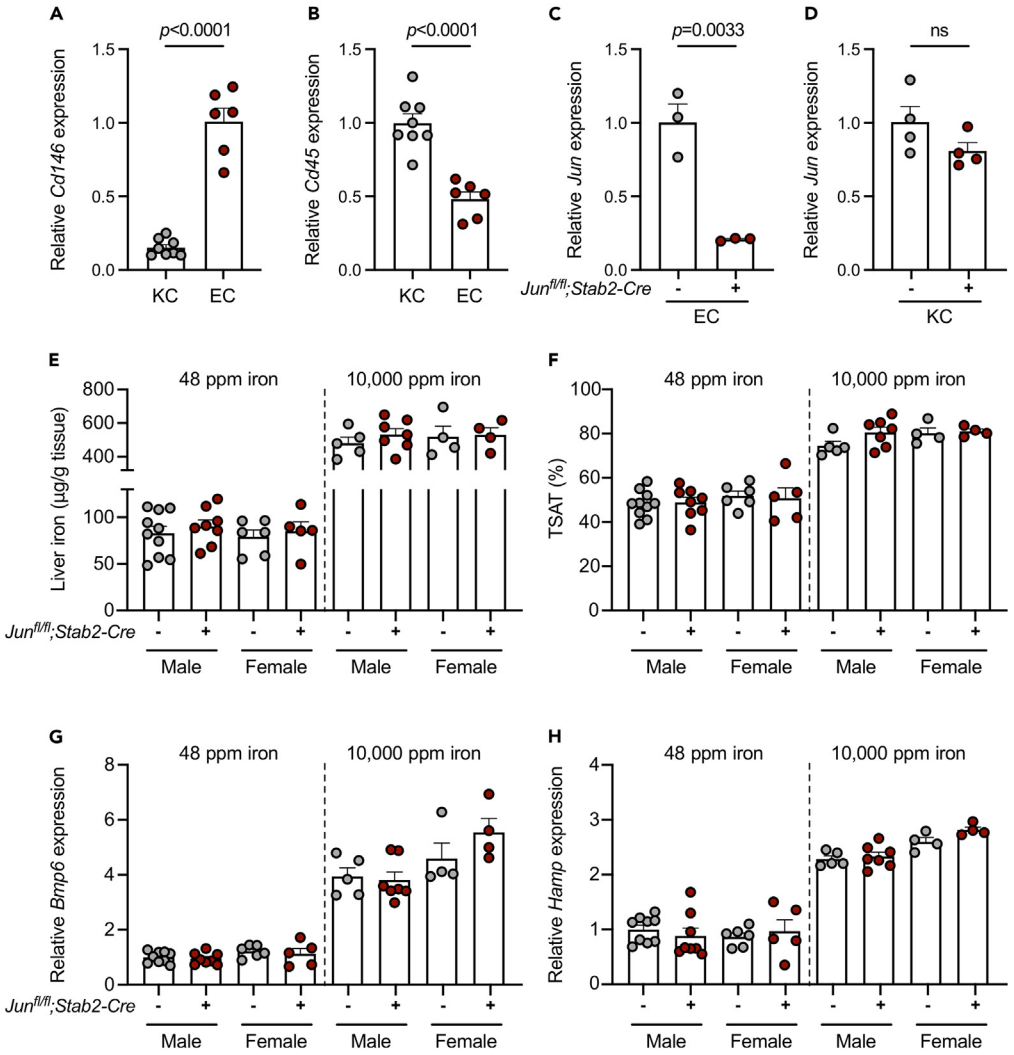

Figure 4. Endothelial *Jun* knockout mice do not exhibit changes in liver *Bmp6* expression or other iron homeostasis parameters

Endothelial cells (EC) and Kupffer cells (KC) were isolated from *Jun*$^{fl/fl}$;*Stab2-Cre*+ and *Cre*- mouse livers by magnetic separation (n = 3–4/group) and analyzed for enrichment by expression of cell-specific markers (A and B) *Cd146* (EC) and *Cd45* (KC), and expression of (C and D) *Jun* relative to *Rpl19* by qRT-PCR in EC and KC, respectively. In panels (A and B), cells from *Cre*+ and *Cre*- mice were combined for purity analysis for a total of n = 6–8/group.

(E–H) Six-week-old male (n = 5–7/group) and female (n = 4/group) *Jun*$^{fl/fl}$;*Stab2-Cre*+ and littermate *Cre*- mice were fed purified iron-sufficient diet (48 ppm iron) or high-iron diet (10,000 ppm iron) for 2 weeks and analyzed at 8 weeks for (E) liver iron concentration, (F) serum transferrin saturation (TSAT), and (G) hepatic expression of *Bmp6* and (H) *Hamp* relative to *Rpl19* by qRT-PCR. Bar graphs represent mean ± SEM with individual points indicating the number of animals. Statistical differences between groups were determined by two-tailed Student's t test for normally distributed values. ns, not significant. See also Figure S5 and Tables S1 and S2.

RNA-sequencing and proteomics of isolated liver endothelial cells. The prior study[16] also used different models of iron loading with short-term single injection of iron-rich holo-transferrin or 18 h feeding of a high-iron diet after pre-treatment with an iron-deficient diet, compared to the long-term 4 weeks feeding of a high-iron diet in our study. Notably, we and others have found that liver *Bmp6* expression is induced by high iron as early as 6 h (depending on the strength of the iron stimulus), peaks at 2 weeks, and persists for as long as 4 weeks,[8,13,16,19,37] suggesting that any pathways involved in iron-mediated *Bmp6* regulation would be expected to be impacted at all of these timepoints. The concordant results between these studies across different unbiased approaches, different models of iron loading, and different labs supports the robustness and reproducibility of the finding that iron induces c-Jun activity in liver endothelial cells in parallel with *Bmp6* under both short-term and long-term iron stimuli.

Members of the Jun family (c-Jun, JunB, and JunD), along with Fos, Atf, or Maf family proteins, form the AP-1 transcription factor complex. The AP-1 transcription factor complex is involved in a variety of cellular processes including proliferation, stress, apoptosis, and transformation.[38,39] In addition to cellular oxidative stress, AP-1 is also suggested to function in regulation of the hemochromatosis gene *HFE*,[40] and, via

c-Jun, transcription of the plasma iron oxidase ceruloplasmin.[41] Interestingly, one study previously reported transcriptional activation of *BMP6* by JunB in endothelial-derived cell cultures.[42] In this study, *BMP6* induction was caused by treatment with the iron chelator 2,2′-dipyridyl; however, *BMP6* induction did not occur with other iron-chelators and was iron-independent.[42] It is important to note that *in vivo*, *Bmp6* expression is decreased rather than induced by iron deficiency.[8,15,37,43] Thus, the biological significance of these findings in regard to iron-mediated BMP6 regulation is unclear.

In this study, we used a primary liver endothelial cell culture system to test whether c-Jun has a functional role in iron-mediated *Bmp6* regulation. We confirmed our previous findings that NTBI can induce *Bmp6* in a cell-autonomous fashion in liver endothelial cells[15,19] and showed that regulation of *Bmp6* expression by NTBI occurs at the transcriptional level. Moreover, we showed that c-Jun regulates *Bmp6* expression by NTBI because *Bmp6* induction was inhibited in *Jun* knockdown cells. Notably, although the ability of iron to induce *Bmp6* in isolated liver endothelial cell cultures is highly reproducible in our hands,[15,19] another group was not able to demonstrate iron-mediated *Bmp6* induction in a different primary liver sinusoidal endothelial cell culture model.[44] This same group was not able to replicate the ability of Nrf-2 activation to induce *Bmp6* in their cell culture model.[44] The different findings may be related to variations in the liver endothelial cell isolation, cell culture procedure, and the use of a different Nrf-2 activator. In contrast to the other group, we did not attempt to isolate sinusoidal liver endothelial cells specifically, rather than a more general liver endothelial cell population, because the specific role for liver sinusoidal endothelial cells in BMP6 production for hepcidin regulation has not been definitively established *in vivo*. One limitation of all primary liver endothelial cell culture models is that these cells lose their functional characteristics very quickly in cell culture. However, we believe that our liver endothelial cell culture is a valid model because the cells retain their endothelial protein markers and the ability to upregulate *Bmp6* in response to iron and the Nrf-2 activator CDDO-Im, similar to what occurs *in vivo*. Nevertheless, these limitations emphasize the importance of further validating liver endothelial cell culture findings using other methods.

To explore whether c-Jun has a direct functional role in *Bmp6* transcription, we utilized publicly available ENCODE data in human umbilical vein endothelial cells (HUVECs) to identify consensus sequence binding sites for c-Jun in predicted regulatory regions of the human *BMP6* gene that are conserved across species. Moreover, ENCODE ChIP sequencing data showed peaks for c-Jun binding at these predicted sites, consistent with an interaction between c-Jun and *BMP6*, at least in this cell culture model. Similar data were previously shown in support of Nrf-2 interacting with murine *Bmp6* in a myoblast cell line.[19] However, the direct interaction of Nrf-2 with *Bmp6* in liver endothelial cells was not experimentally validated in the prior study,[19] nor its dependence on iron. Here, we confirmed c-Jun binding to murine *Bmp6* regulatory regions by ChIP-qPCR in whole livers in an iron-dependent fashion. Interestingly, although one of the confirmed binding sites contained a c-Jun consensus binding motif consistent with direct DNA binding, c-Jun also bound to the *Bmp6* promoter where a consensus binding motif was not identified. It is possible that c-Jun interaction with the *Bmp6* promoter occurs through an atypical c-Jun binding motif or is indirect via an interaction with another transcription factor. Future studies are needed to clarify where and how c-Jun binds to the *Bmp6* promoter region. It is expected that endothelial cells are the most likely cell type in which this binding occurs due to their preferential production of BMP6 compared with other liver cell populations[8,9] as well as results from the integrative omics analysis and ENCODE ChIP sequencing data. However, which liver cell populations exhibit binding activity was not definitively determined, as we were unable to utilize sorted endothelial cells due to a lack of sufficient starting material or downstream interference from antibody-based isolation methods.

In our model, we were unable to confirm c-Jun binding to the *Bmp6* intron 1 region, which contains a consensus c-Jun binding sequence and where c-Jun binding was detected in ENCODE ChIP sequencing data. This could be due to the use of different model systems—HUVECs for the ENCODE ChIP sequencing data versus whole mouse livers in our experiment. It is also possible that technical limitations precluded our ability to detect this interaction. Our ChIP-qPCR experiments were technically challenging because we used whole liver tissue rather than a cell culture system and because reliable reagents to detect mouse c-Jun are limited. We found differences in binding with the negative IgG antibody and background amplification among different dietary iron conditions, including a very high IgG background in mice fed the high-iron diet. It is for these reasons that we designed our study to compare abundance relative to the IgG negative control within each dietary group rather than between dietary groups, and we included only iron-deficient diet and iron-sufficient diet groups to explore iron-dependence of the binding. Despite these technical challenges, our findings, together with the publicly available ENCODE ChIP sequencing data, support the conclusion that c-Jun binds to *Bmp6* regulatory regions, and this binding appears to be iron-dependent.

Importantly, we found that blocking c-Jun phosphorylation using a broad-spectrum JNK inhibitor disrupted the iron homeostatic response to dietary iron loading *in vivo* by inhibiting the induction of *Bmp6, Bmp2,* and hepcidin. Mechanistically, based on the RNA-seq and proteomics data, liver endothelial cell culture studies, ENCODE ChIP sequencing data, and ChIP-qPCR experiments, we hypothesize that inhibiting c-Jun had a direct effect to inhibit *Bmp6* transcriptional regulation by iron in liver endothelial cells, resulting in the hepcidin decrease. However, the lack of specificity of the inhibitor for c-Jun alone, and its global activity when administered parenterally do not definitively demonstrate an exclusive and independent role for c-Jun in regulating *Bmp6* in endothelial cells in mice. Whether *Bmp2* induction by iron may also be controlled directly by c-Jun remains to be determined. Iron failed to induce *Bmp2* mRNA in the liver endothelial cell culture system[15] precluding *in vitro* validation using this model. Although JNK inhibition reduced hepcidin expression, this had no effect on systemic iron levels. It is possible that this is related to the short time course of the experiment, or modest degree of *Bmp6* and hepcidin suppression that may not be enough to induce iron loading at the time point examined. It is also possible that counter regulation of iron levels by hepcidin already occurred, and iron levels would have been different at an earlier time point after JNK inhibitor treatment. Lastly, it is also possible that the JNK inhibitor has additional impacts on other aspects of iron regulation that counteract the effects of BMP6 and hepcidin.

To address the question of c-Jun function to regulate *Bmp6* specifically in endothelial cells *in vivo*, we generated mice that lack endothelial *Jun* using the *Stabilin2-Cre* driver, which has restricted activity to primarily sinusoidal endothelial cells in the liver, spleen, and bone marrow,

with minor activity in some hematopoietic cell populations (<10%) and resident liver macrophages (≤25%).[10,15,31] We did not find any notable differences in *Bmp6* expression, hepcidin expression, or other iron homeostasis parameters when analyzing endothelial *Jun* knockout animals under baseline or high-iron conditions. This finding does not rule out a functional role for c-Jun in mediating iron-dependent *Bmp6* regulation in liver endothelial cells, which is supported by many other lines of evidence in this study. It is possible that there is compensatory or antagonistic regulation from other members of the Jun family (JunB or JunD), that could obscure any differences in single endothelial *Jun* knockout mice. For example, knock-in of *JunB* was shown to rescue both liver and cardiac defects seen in global *Jun* knockout animals, which are otherwise lethal.[45] Additionally, conditional epidermal deletion of both *Jun* and *JunB* caused a psoriasis-like skin phenotype, whereas deletion of either *Jun* or *JunB* alone did not.[46] Similar to what occurs in epidermal cells, the expression of genes like *Bmp6* in endothelial cells could be regulated equally by c-Jun and JunB, or JunD. Recently, transactivation of *BMP6* in an iron-independent setting was demonstrated to involve JunB, further supporting this possibility.[42] Although this potential redundancy did not preclude our detecting a functional role for c-Jun in isolated liver endothelial cell culture experiments, it is possible that compensation may not occur in cell culture studies due to the short-term and/or incomplete nature of the knockdown in this model system. Considering that all Jun family members can participate in the oxidative stress response,[26] and JunB can regulate *Bmp6* expression in other settings,[42] future studies of double or triple endothelial *Jun*, *JunB*, and *JunD* knockout animals may more clearly establish an *in vivo* functional role for the Jun transcription factor pathway in endothelial cell *Bmp6* regulation by iron and distinguish the regulatory contribution of each Jun family member.

A second potential explanation for the lack of phenotype in the endothelial *Jun* knockout mice is that c-Jun may have a functional role in additional cell types, such as neighboring hepatocytes. Of note, hepatocytes rapidly take up and accumulate NTBI, and specifically utilize the c-Jun pathway to protect against other types of cellular stress.[47] Detailed co-culture studies of liver endothelial cells and hepatocytes or other liver cell populations would provide insight into other potential functions of c-Jun, which are not apparent in isolated liver endothelial cell culture studies. Notably, the prior study demonstrating a functional impact of the Nrf-2 pathway in *Bmp6* regulation was performed in global knockout animals.[19] Thus the effects in that model could also be partially due to signals from other cell types, in addition to endothelial cells. It is possible we would detect alteration of iron-mediated *Bmp6* regulation in global *Jun* deficient animals, similar to what occurs in JNK inhibitor treated mice or global *Nfe2l2* knockout mice. However, these studies are precluded by the embryonic lethality of germline *Jun* deletion.[48] Future studies using an inducible global *Jun* knockout mouse model may be useful in further understanding the role of c-Jun in *Bmp6* regulation by iron *in vivo*.

To understand whether and how the c-Jun pathway may crosstalk with the Nrf-2 pathway in *Bmp6* regulation, we investigated the impact of c-Jun inhibition on Nrf-2 activation in our different model systems. The fact that *Bmp6* expression was decreased by *Jun* knockdown or JNK inhibition despite an induction of other Nrf-2 pathway targets confirms that Nrf-2 is not the sole mediator of *Bmp6* regulation by iron and that c-Jun is not regulating *Bmp6* indirectly by impacting the Nrf-2 pathway. Moreover, the ability of CDDO-Im to induce Nrf-2 activity and *Bmp6* irrespective of endothelial *Jun* knockdown or knockout, demonstrates that Nrf-2 does not require endothelial c-Jun to regulate *Bmp6*. Overall, these data are consistent with nonoverlapping effects of c-Jun and Nrf-2 in *Bmp6* regulation, but a full understanding of potential crosstalk between these pathways will require further study.

In summary, we have generated the first comprehensive analysis of transcriptomic and proteomic responses to iron loading in liver endothelial cells, which have uncovered a novel functional role for the c-Jun transcription factor pathway in regulating *Bmp6* transcription in high iron conditions, independent of Nrf-2 pathway activation. However, the role of c-Jun may be genetically redundant with other members of the Jun family and/or may require coordinated activity in multiple cell types. These findings provide important new insights into how endothelial cells sense iron levels to regulate systemic iron homeostasis, which may ultimately pave the way for new treatments for iron overload disorders.

Limitations of the study

The collective results from our study suggest a functional role for the c-Jun transcription factor pathway in *Bmp6* transcriptional regulation in response to iron. However, our study has several limitations. First, we used different timings of feeding high-iron diets for different experiments. Although *Bmp6* expression is increased by the high-iron diet in all dietary models, the different timings make direct comparisons between the experimental results difficult. Second, although our primary liver endothelial cell cultures do retain several of their important *in vivo* characteristics, including iron-mediated *Bmp6* responsiveness, it is uncertain how faithfully this cell culture model recapitulates all of the functions of these cells *in vivo*. Third, we had technical limitations in our ChIP-qPCR experiments, including differences in background IgG binding in different dietary iron groups, which precluded our ability to assess binding in the high-iron diet group or compare binding across iron diets. Moreover, we were not able to confirm c-Jun binding to the intron 1 region of *Bmp6* where there is a known consensus site and c-Jun interaction was previously demonstrated by ChIP-seq in HUVECs. Finally, we could not definitively determine a functional role for endothelial c-Jun in *Bmp6* regulation to control iron homeostasis *in vivo* due to potential global or off target effects of the JNK inhibitor, and lack of phenotype in endothelial *Jun* knockout mice, which may be due to redundancy with other Jun family members or may require coordinated activity in multiple cell types.

STAR★METHODS

Detailed methods are provided in the online version of this paper and include the following:

- KEY RESOURCES TABLE
- RESOURCE AVAILABILITY
  - Lead contact
  - Materials availability

SUPPLEMENTAL INFORMATION

Supplemental information can be found online at https://doi.org/10.1016/j.isci.2023.108555.

ACKNOWLEDGMENTS

The authors thank the Harvard Stem Cell Institute-Center for Regenerative Medicine Flow Cytometry Core Facility for performing cell sorting, the MGH NextGen Sequencing Core for performing RNA-Seq, the MGH Center for Comparative Medicine Clinical Pathology Laboratory for blood analyses. The authors thank Manfred Nairz for help in setting up the cell sorting protocol, Adhvaith Sridhar for technical assistance with the CDDO-Im gavage experiments, and the ENCODE consortium for generating the ChIP-Seq datasets. This study was supported by the National Institutes of Health grants T32-DK007540 (to ALF), R01-DK087727 and R01-DK128068 (to JLB), R01-DK124384 (to JDM), and the Patricia and Scott Eston Massachusetts General Hospital Research Scholar Award (to JLB).

AUTHOR CONTRIBUTIONS

A.L.F. performed experiments, analyzed data, and wrote the manuscript. C.Y.W., Y.X., S.P., and X.X. performed experiments and analyzed data. J.A.P. and J.D.M. performed proteomics and analyzed data. B.M. and W.F. performed GSEA analysis and analyzed data. J.L.B. conceived and designed the project and wrote the manuscript. All authors commented on the manuscript.

DECLARATION OF INTERESTS

J.L.B. has been a consultant for Incyte Corporation and Alnylam Pharmaceuticals, and owned equity in Ferrumax Pharmaceuticals, a company focused on targeting RGM proteins (including hemojuvelin) and bone morphogenetic protein (BMP/TGF-beta) superfamily signaling as hepcidin modulating agents for the treatment of anemia and other iron disorders. J.B.L.s interests were reviewed and are managed by Massachusetts General Hospital and Mass General Brigham in accordance with their conflict-of-interest policies. C.Y.W. is currently employed at Keros Therapeutics, Lexington, MA, USA, and Y.X. is currently employed at Moderna Therapeutics, Cambridge, MA, USA. The other authors declare no conflict of interest.

Received: February 17, 2023
Revised: September 29, 2023
Accepted: November 20, 2023
Published: November 22, 2023

REFERENCES

1. Nemeth, E., Tuttle, M.S., Powelson, J., Vaughn, M.B., Donovan, A., Ward, D.M., Ganz, T., and Kaplan, J. (2004). Hepcidin Regulates Cellular Iron Efflux by Binding to Ferroportin and Inducing Its Internalization. Science *306*, 2090–2093.
2. Ganz, T., Olbina, G., Girelli, D., Nemeth, E., and Westerman, M. (2008). Immunoassay for human serum hepcidin. Blood *112*, 4292–4297.
3. Fisher, A.L., and Nemeth, E. (2017). Iron homeostasis during pregnancy. Am. J. Clin. Nutr. *106*, 1567s–1574s.
4. Nemeth, E., Valore, E.V., Territo, M., Schiller, G., Lichtenstein, A., and Ganz, T. (2003). Hepcidin, a putative mediator of anemia of inflammation, is a type II acute-phase protein. Blood *101*, 2461–2463.
5. Nemeth, E., Rivera, S., Gabayan, V., Keller, C., Taudorf, S., Pedersen, B.K., and Ganz, T. (2004). IL-6 mediates hypoferremia of inflammation by inducing the synthesis of the iron regulatory hormone hepcidin. J. Clin. Invest. *113*, 1271–1276.

6. Camaschella, C., Nai, A., and Silvestri, L. (2020). Iron metabolism and iron disorders revisited in the hepcidin era. Haematologica *105*, 260–272.
7. Fisher, A.L., and Babitt, J.L. (2022). Coordination of iron homeostasis by bone morphogenetic proteins: Current understanding and unanswered questions. Dev. Dyn. *251*, 26–46.
8. Canali, S., Wang, C.Y., Zumbrennen-Bullough, K.B., Bayer, A., and Babitt, J.L. (2017). Bone morphogenetic protein 2 controls iron homeostasis in mice independent of Bmp6. Am. J. Hematol. *92*, 1204–1213.
9. Canali, S., Zumbrennen-Bullough, K.B., Core, A.B., Wang, C.Y., Nairz, M., Bouley, R., Swirski, F.K., and Babitt, J.L. (2017). Endothelial cells produce bone morphogenetic protein 6 required for iron homeostasis in mice. Blood *129*, 405–414.
10. Koch, P.S., Olsavszky, V., Ulbrich, F., Sticht, C., Demory, A., Leibing, T., Henzler, T., Meyer, M., Zierow, J., Schneider, S., et al. (2017). Angiocrine Bmp2 signaling in murine liver controls normal iron homeostasis. Blood *129*, 415–419.
11. Kautz, L., Besson-Fournier, C., Meynard, D., Latour, C., Roth, M.P., and Coppin, H. (2011). Iron overload induces BMP6 expression in the liver but not in the duodenum. Haematologica *96*, 199–203.
12. Wang, C.Y., Canali, S., Bayer, A., Dev, S., Agarwal, A., and Babitt, J.L. (2019). Iron, erythropoietin, and inflammation regulate hepcidin in Bmp2-deficient mice, but serum iron fails to induce hepcidin in Bmp6-deficient mice. Am. J. Hematol. *94*, 240–248.
13. Corradini, E., Meynard, D., Wu, Q., Chen, S., Ventura, P., Pietrangelo, A., and Babitt, J.L. (2011). Serum and liver iron differently regulate the bone morphogenetic protein 6 (BMP6)-SMAD signaling pathway in mice. Hepatology *54*, 273–284.
14. Xiao, X., Dev, S., Canali, S., Bayer, A., Xu, Y., Agarwal, A., Wang, C.-Y., and Babitt, J.L. (2020). Endothelial Bone Morphogenetic Protein 2 (Bmp2) Knockout Exacerbates Hemochromatosis in Homeostatic Iron Regulator (Hfe) Knockout Mice but not Bmp6 Knockout Mice. Hepatology *72*, 642–655.
15. Fisher, A.L., Wang, C.Y., Xu, Y., Joachim, K., Xiao, X., Phillips, S., Moschetta, G.A., Alfaro-Magallanes, V.M., and Babitt, J.L. (2022). Functional role of endothelial transferrin receptor 1 in iron sensing and homeostasis. Am. J. Hematol. *97*, 1548–1559.
16. Charlebois, E., Fillebeen, C., Presley, J., Cagnone, G., Lisi, V., Lavallée, V.P., Joyal, J.-S., and Pantopoulos, K. (2023). Liver sinusoidal endothelial cells induce BMP6 expression in response to non–transferrin-bound iron. Blood *141*, 271–284.
17. Chua, A.C.G., Drake, S.F., Herbison, C.E., Olynyk, J.K., Leedman, P.J., and Trinder, D. (2006). Limited iron export by hepatocytes contributes to hepatic iron-loading in the Hfe knockout mouse. J. Hepatol. *44*, 176–182.
18. Knutson, M.D. (2019). Non-transferrin-bound iron transporters. Free Radic. Biol. Med. *133*, 101–111.
19. Lim, P.J., Duarte, T.L., Arezes, J., Garcia-Santos, D., Hamdi, A., Pasricha, S.R., Armitage, A.E., Mehta, H., Wideman, S., Santos, A.G., et al. (2019). Nrf2 controls iron homeostasis in haemochromatosis and thalassaemia via Bmp6 and hepcidin. Nat. Metab. *1*, 519–531.
20. Luo, Y., Hitz, B.C., Gabdank, I., Hilton, J.A., Kagda, M.S., Lam, B., Myers, Z., Sud, P., Jou, J., Lin, K., et al. (2020). New developments on the Encyclopedia of DNA Elements (ENCODE) data portal. Nucleic Acids Res. *48*. D882-d889.
21. ENCODE Project Consortium (2012). An integrated encyclopedia of DNA elements in the human genome. Nature *489*, 57–74.
22. Evans, R.W., Rafique, R., Zarea, A., Rapisarda, C., Cammack, R., Evans, P.J., Porter, J.B., and Hider, R.C. (2008). Nature of non-transferrin-bound iron: studies on iron citrate complexes and thalassemic sera. J. Biol. Inorg. Chem. *13*, 57–74.
23. Grootveld, M., Bell, J.D., Halliwell, B., Aruoma, O.I., Bomford, A., and Sadler, P.J. (1989). Non-transferrin-bound iron in plasma or serum from patients with idiopathic hemochromatosis. Characterization by high performance liquid chromatography and nuclear magnetic resonance spectroscopy. J. Biol. Chem. *264*, 4417–4422.
24. Gozzelino, R., and Soares, M.P. (2014). Coupling heme and iron metabolism via ferritin H chain. Antioxid. Redox Signal. *20*, 1754–1769.
25. Kamata, H., Honda, S.I., Maeda, S., Chang, L., Hirata, H., and Karin, M. (2005). Reactive oxygen species promote TNFalpha-induced death and sustained JNK activation by inhibiting MAP kinase phosphatases. Cell *120*, 649–661.
26. Venugopal, R., and Jaiswal, A.K. (1998). Nrf2 and Nrf1 in association with Jun proteins regulate antioxidant response element-mediated expression and coordinated induction of genes encoding detoxifying enzymes. Oncogene *17*, 3145–3156.
27. Kunsch, C., and Medford, R.M. (1999). Oxidative stress as a regulator of gene expression in the vasculature. Circ. Res. *85*, 753–766.
28. Sen, C.K., and Packer, L. (1996). Antioxidant and redox regulation of gene transcription. FASEB J *10*, 709–720.
29. Bennett, B.L., Sasaki, D.T., Murray, B.W., O'Leary, E.C., Sakata, S.T., Xu, W., Leisten, J.C., Motiwala, A., Pierce, S., Satoh, Y., et al. (2001). SP600125, an anthrapyrazolone inhibitor of Jun N-terminal kinase. Proc. Natl. Acad. Sci. USA *98*, 13681–13686.
30. Behrens, A., Sibilia, M., David, J.P., Möhle-Steinlein, U., Tronche, F., Schütz, G., and Wagner, E.F. (2002). Impaired postnatal hepatocyte proliferation and liver regeneration in mice lacking c-jun in the liver. EMBO J *21*, 1782–1790.
31. Géraud, C., Koch, P.-S., Zierow, J., Klapproth, K., Busch, K., Olsavszky, V., Leibing, T., Demory, A., Ulbrich, F., Diett, M., et al. (2017). GATA4-dependent organ-specific endothelial differentiation controls liver development and embryonic hematopoiesis. J. Clin. Invest. *127*, 1099–1114.
32. Andriopoulos, B., Jr., Corradini, E., Xia, Y., Faasse, S.A., Chen, S., Grgurevic, L., Knutson, M.D., Pietrangelo, A., Vukicevic, S., Lin, H.Y., and Babitt, J.L. (2009). BMP6 is a key endogenous regulator of hepcidin expression and iron metabolism. Nat. Genet. *41*, 482–487.
33. Meynard, D., Kautz, L., Darnaud, V., Canonne-Hergaux, F., Coppin, H., and Roth, M.P. (2009). Lack of the bone morphogenetic protein BMP6 induces massive iron overload. Nat. Genet. *41*, 478–481.
34. Piubelli, C., Castagna, A., Marchi, G., Rizzi, M., Busti, F., Badar, S., Marchetti, M., De Gobbi, M., Roetto, A., Xumerle, L., et al. (2017). Identification of new BMP6 pro-peptide mutations in patients with iron overload. Am. J. Hematol. *92*, 562–568.
35. Daher, R., Kannengiesser, C., Houamel, D., Lefebvre, T., Bardou-Jacquet, E., Ducrot, N., de Kerguenec, C., Jouanolle, A.M., Robreau, A.M., Oudin, C., et al. (2016). Heterozygous Mutations in BMP6 Pro-peptide Lead to Inappropriate Hepcidin Synthesis and Moderate Iron Overload in Humans. Gastroenterology *150*, 672–683.e4.
36. Corradini, E., Schmidt, P.J., Meynard, D., Garuti, C., Montosi, G., Chen, S., Vukicevic, S., Pietrangelo, A., Lin, H.Y., and Babitt, J.L. (2010). BMP6 treatment compensates for the molecular defect and ameliorates hemochromatosis in Hfe knockout mice. Gastroenterology *139*, 1721–1729.
37. Kautz, L., Meynard, D., Monnier, A., Darnaud, V., Bouvet, R., Wang, R.H., Deng, C., Vaulont, S., Mosser, J., Coppin, H., and Roth, M.P. (2008). Iron regulates phosphorylation of Smad1/5/8 and gene expression of Bmp6, Smad7, Id1, and Atoh8 in the mouse liver. Blood *112*, 1503–1509.
38. Shaulian, E., and Karin, M. (2002). AP-1 as a regulator of cell life and death. Nat. Cell Biol. *4*, E131–E136.
39. Eferl, R., and Wagner, E.F. (2003). AP-1: a double-edged sword in tumorigenesis. Nat. Rev. Cancer *3*, 859–868.
40. Sánchez, M., Queralt, R., Bruguera, M., Rodés, J., and Oliva, R. (1998). Cloning, sequencing and characterization of the rat hereditary hemochromatosis promoter: comparison of the human, mouse and rat HFE promoter regions. Gene *225*, 77–87.
41. Das, D., Tapryal, N., Goswami, S.K., Fox, P.L., and Mukhopadhyay, C.K. (2007). Regulation of ceruloplasmin in human hepatic cells by redox active copper: identification of a novel AP-1 site in the ceruloplasmin gene. Biochem. J. *402*, 135–141.
42. Noguchi, T., Ikeda, M., Murakami, M., Masuzawa, M., Imamura, T., Hashimoto, O., Matsui, T., and Funaba, M. (2020). Regulatory expression of bone morphogenetic protein 6 by 2,2′-dipyridyl. Biochim. Biophys. Acta. Gen. Subj. *1864*, 129610.
43. Finberg, K.E., Whittlesey, R.L., Fleming, M.D., and Andrews, N.C. (2010). Down-regulation of Bmp/Smad signaling by Tmprss6 is required for maintenance of systemic iron homeostasis. Blood *115*, 3817–3826.
44. Colucci, S., Altamura, S., Marques, O., Müdder, K., Agarvas, A.R., Hentze, M.W., and Muckenthaler, M.U. (2022). Iron-dependent BMP6 Regulation in Liver Sinusoidal Endothelial Cells Is Instructed by Hepatocyte-derived Secretory Signals. Hemasphere *6*, e773.
45. Passegué, E., Jochum, W., Behrens, A., Ricci, R., and Wagner, E.F. (2002). JunB can substitute for Jun in mouse development and cell proliferation. Nat. Genet. *30*, 158–166.
46. Zenz, R., Eferl, R., Kenner, L., Florin, L., Hummerich, L., Mehic, D., Scheuch, H., Angel, P., Tschachler, E., and Wagner, E.F. (2005). Psoriasis-like skin disease and arthritis caused by inducible epidermal deletion of Jun proteins. Nature *437*, 369–375.
47. Fuest, M., Willim, K., MacNelly, S., Fellner, N., Resch, G.P., Blum, H.E., and Hasselblatt, P. (2012). The transcription factor c-Jun protects against sustained hepatic endoplasmic reticulum stress thereby promoting hepatocyte survival. Hepatology *55*, 408–418.

48. Hilberg, F., Aguzzi, A., Howells, N., and Wagner, E.F. (1993). c-jun is essential for normal mouse development and hepatogenesis. Nature *365*, 179–181.
49. Edgar, R., Domrachev, M., and Lash, A.E. (2002). Gene Expression Omnibus: NCBI gene expression and hybridization array data repository. Nucleic Acids Res. *30*, 207–210.
50. Perez-Riverol, Y., Bai, J., Bandla, C., García-Seisdedos, D., Hewapathirana, S., Kamatchinathan, S., Kundu, D.J., Prakash, A., Frericks-Zipper, A., Eisenacher, M., et al. (2022). The PRIDE database resources in 2022: a hub for mass spectrometry-based proteomics evidences. Nucleic Acids Res. *50*. D543-d552.
51. Paulo, J.A., Gaun, A., and Gygi, S.P. (2015). Global Analysis of Protein Expression and Phosphorylation Levels in Nicotine-Treated Pancreatic Stellate Cells. J. Proteome Res. *14*, 4246–4256.
52. McAlister, G.C., Nusinow, D.P., Jedrychowski, M.P., Wühr, M., Huttlin, E.L., Erickson, B.K., Rad, R., Haas, W., and Gygi, S.P. (2014). MultiNotch MS3 Enables Accurate, Sensitive, and Multiplexed Detection of Differential Expression across Cancer Cell Line Proteomes. Anal. Chem. *86*, 7150–7158.
53. Ting, L., Rad, R., Gygi, S.P., and Haas, W. (2011). MS3 eliminates ratio distortion in isobaric multiplexed quantitative proteomics. Nat. Methods *8*, 937–940.
54. Beausoleil, S.A., Villén, J., Gerber, S.A., Rush, J., and Gygi, S.P. (2006). A probability-based approach for high-throughput protein phosphorylation analysis and site localization. Nat. Biotechnol. *24*, 1285–1292.
55. Huttlin, E.L., Jedrychowski, M.P., Elias, J.E., Goswami, T., Rad, R., Beausoleil, S.A., Villén, J., Haas, W., Sowa, M.E., and Gygi, S.P. (2010). A tissue-specific atlas of mouse protein phosphorylation and expression. Cell *143*, 1174–1189.
56. Elias, J.E., and Gygi, S.P. (2010). Target-decoy search strategy for mass spectrometry-based proteomics. Methods Mol. Biol. *604*, 55–71.
57. Elias, J.E., and Gygi, S.P. (2007). Target-decoy search strategy for increased confidence in large-scale protein identifications by mass spectrometry. Nat. Methods *4*, 207–214.
58. McAlister, G.C., Huttlin, E.L., Haas, W., Ting, L., Jedrychowski, M.P., Rogers, J.C., Kuhn, K., Pike, I., Grothe, R.A., Blethrow, J.D., and Gygi, S.P. (2012). Increasing the multiplexing capacity of TMTs using reporter ion isotopologues with isobaric masses. Anal. Chem. *84*, 7469–7478.
59. Nassar, L.R., Barber, G.P., Benet-Pagès, A., Casper, J., Clawson, H., Diekhans, M., Fischer, C., Gonzalez, J.N., Hinrichs, A.S., Lee, B.T., et al. (2023). The UCSC Genome Browser database: 2023 update. Nucleic Acids Res. *51*, D1188–D1195.
60. Lander, E.S., Linton, L.M., Birren, B., Nusbaum, C., Zody, M.C., Baldwin, J., Devon, K., Dewar, K., Doyle, M., FitzHugh, W., et al. (2001). Initial sequencing and analysis of the human genome. Nature *409*, 860–921.
61. Kent, W.J., Sugnet, C.W., Furey, T.S., Roskin, K.M., Pringle, T.H., Zahler, A.M., and Haussler, D. (2002). The human genome browser at UCSC. Genome Res. *12*, 996–1006.
62. Torrance, J.D., and Bothwell, T.H. (1968). A simple technique for measuring storage iron concentrations in formalinised liver samples. S. Afr. J. Med. Sci. *33*, 9–11.

STAR★METHODS

KEY RESOURCES TABLE

REAGENT or RESOURCEs	SOURCE	IDENTIFIER
Antibodies		
Goat polyclonal anti-ferritin light chain	Novus Biologicals	Cat#Nbp1-06986; RRID: AB_2294316
Rabbit monoclonal anti-cJun	Cell Signaling Technology	Cat#9165; RRID: AB_2130165
Mouse monoclonal anti-β-actin	Millipore Sigma	Cat#MAB1501; RRID: AB_2223041
Donkey polyclonal anti-goat-HRP	Jackson Immunoresearch	Cat#705-036-147; RRID: AB_2340392
Donkey polyclonal anti-rabbit-HRP	GE Healthcare Life Sciences	Cat#NA9340; RRID: AB_772191
Goat polyclonal anti-mouse-HRP	Jackson Immunoresearch	Cat#115-035-003; RRID: AB_10015289
Rabbit polyclonal anti-cJun	Abcam	Cat#ab31419; RRID: AB_731605
Normal rabbit polyclonal IgG	Cell Signaling Technology	Cat#2729; RRID: AB_1031062
Rabbit monoclonal anti-H3K4me3	Millipore Sigma	Cat#04-745; RRID: AB_1163444
Rat monoclonal FITC anti-mouse Ly-6C	Biolegend	Cat#128006; RRID: AB_1186135
Rat monoclonal PE anti-mouse CD146	Biolegend	Cat#134704; RRID: AB_2143527
Mouse monoclonal PerCP/Cyanine5.5 anti-mouse CD64	Biolegend	Cat#139307; RRID: AB_2561962
Rat monoclonal PE/Cyanine7 anti-mouse F4/80	Biolegend	Cat#123114; RRID: AB_893478
Mouse monoclonal Pacific Blue anti-mouse CD45.2	Biolegend	Cat#109820; RRID: AB_492872
Rat monoclonal Brilliant Violet 605 anti-mouse CD31	Biolegend	Cat#102427; RRID: AB_2563982
Armenian hamster monoclonal APC anti-mouse CD3ε	Biolegend	Cat#100312; RRID: AB_312677
Rat monoclonal APC anti-mouse CD19	Biolegend	Cat#115512; RRID: AB_313647
Rat monoclonal APC anti-mouse CD90.2	Biolegend	Cat#140312; RRID: AB_10640728
Rat monoclonal APC anti-mouse CD326	Biolegend	Cat#118214; RRID: AB_1134102
Rat monoclonal APC anti-mouse Ly-6G	Biolegend	Cat#127613; RRID: AB_1877163
Mouse monoclonal APC anti-mouse NK-1.1	Biolegend	Cat#108709; RRID: AB_313396
Rat monoclonal Alexa Fluor 700 anti-mouse MCH class II	eBioscience	Cat#56-5321-80; RRID: AB_494009
Rat monoclonal APC/Cyanine7 anti-mouse CD11b	Biolegend	Cat#101226; RRID: AB_830642
Mouse CD-146 microbeads	Miltenyi Biotec	Cat#130-092-007
Mouse F4/80 microbeads	Miltenyi Biotec	Cat#130-110-443
Chemicals, peptides, and recombinant proteins		
c-Jun N-terminal kinase (JNK) inhibitor SP600125	Tocris Bioscience	Cat#1496; CAS: 129-56-6
Nrf-2 activator CDDO-Im	R&D Systems	Cat#4737; CAS: 443104-02-7
Ferric ammonium citrate	Sigma-Aldrich	Cat#F5879; CAS: 1185-57-5
Liver dissociation kit, mouse	Miltenyi Biotec	Cat#130-105-807
Lipofectamine RNAiMAX	Invitrogen	Cat#13778075
PowerUp SYBR Green Master Mix	Applied Biosystems	Cat#A25778
Standard rodent chow (380 ppm iron)	LabDiet	Prolab RMH3000
AIN-93G iron-sufficient diet (37 ppm ferric iron citrate)	Research Diets	Cat#D08090806
AIN-93G high-iron diet (10,000 ppm carbonyl iron)	Research Diets	Cat#D08090805
Iron-deficient diet (2–6 ppm background iron)	Envigo-Teklad	Cat#TD.80396
Iron-sufficient diet (48 ppm ferric iron citrate)	Envigo-Teklad	Cat#TD.80394
High-iron diet (10,000 ppm carbonyl iron)	Envigo-Teklad	Cat#TD.08043
High-iron diet (20,000 ppm carbonyl iron)	Envigo-Teklad	Cat#TD.08496

(*Continued on next page*)

Continued

REAGENT or RESOURCEs	SOURCE	IDENTIFIER
Critical commercial assays		
Perl's iron stain kit	American MasterTech	Cat#KTIRO
TUNEL assay kit	Cell Signaling Technology	Cat#25879
Iron/TIBC kit	Pointe Scientific	Cat#I750460
PicoPure RNA isolation kit	Applied Biosystems	Cat#KIT0204
SuperScript VILO cDNA synthesis kit	Invitrogen	Cat#11754050
High-Capacity RNA-to-cDNA kit	Applied Biosystems	Cat#4387406
RNAeasy Mini kit	Qiagen	Cat#74104
RNAeasy Micro kit	Qiagen	Cat#74004
Pure-Link RNA Mini kit	Invitrogen	Cat#12183025
High pH Reversed-Phase Peptide Fractionation Kit	Pierce	Cat#84868
DC-protein assay kit	Bio-RAD	Cat#5000112
Deposited data		
RNA-sequencing data	This paper	GEO: GSE223871
Quantitative proteomics data	This paper	PRIDE: PXD039830
ChIP-sequencing data	ENCODE	ENCODE: ENCSR000ALG, ENCSR578QSO, ENCSR000ALB, ENCSR000EFA, ENCSR000EOQ
Human reference genome NCBI build 38, GRCh38	Genome Reference Consortium	http://www.ncbi.nlm.nih.gov/projects/genome/assembly/grc/human/
Experimental models: Cell lines		
Primary liver endothelial cells from CD-1 mice	Cell Biologics	Cat#CD-1017
Experimental models: Organisms/strains		
129S6/SvEvTac mice	Taconic Farms	Cat#129SVE
C57BL/6N mice	Taconic Farms	Cat#B6
Jun-floxed mice (C57BL/6)	Richard Libby	Behrens et al.[30]
Stabilin2-Cre mice (C57BL/6)	Cyrill Géraud	Géraud et al.[31]
Conditional endothelial-specific $Jun^{f/f}$;*Stabilin2-Cre* mice (C57BL/6)	This paper	N/A
Oligonucleotides		
Silencer™ Select Negative Control No. 2 siRNA	Invitrogen	Cat#4390846
siGENOME non-targeting siRNA control pool #1	Dharmacon	Cat#D-001206-13-05
Mouse *Jun* siRNA	Invitrogen	Cat#s68564
siGENOME Mouse Jun siRNA - SMARTpool	Dharmacon	Cat#M-043776-01-0005
For qRT-PCR gene-specific primers, see Table S4	This paper	N/A
For ChIP-qRT-PCR primers, see Table S4	This paper	N/A
Software and algorithms		
Prism 9.0	GraphPad	https://www.graphpad.com/
UCSC genome browser	UCSC Genomics Institute	http://genome.ucsc.edu
Agilent 2100 Expert	Agilent	https://www.agilent.com/
GeneSys G:Box Mini 6 (v1.6.1.0)	Syngene	https://www.syngene.com/
QuantStudio3 (v.1.5.1)	Applied Biosystems	https://www.thermofisher.com/
GSEA Desktop (v2.2)	GSEA	https://www.gsea-msigdb.org/gsea/index.jsp
MSigDB geneset (c3.tft.v5.2)	MSigDB	https://www.gsea-msigdb.org/gsea/index.jsp
ImageJ	NIH	https://imagej.net/
CorelDRAW	Corel	https://www.coreldraw.com/

RESOURCE AVAILABILITY

Lead contact

Further information and requests for resources and reagents should be directed to and will be fulfilled by the lead contact, Jodie L Babitt MD (Babitt.jodie@mgh.harvard.edu).

Materials availability

This study did not generate new unique reagents.

Data and code availability

- The RNA-Sequencing data that support the findings of this study have been deposited in the NCBI Gene Expression Omnibus[49] and are accessible through the GEO Series accession number GEO: GSE223871. The mass spectrometry proteomics data that support the findings of this study have been deposited to the ProteomeXchange Consortium via the PRIDE partner repository[50] with the dataset identifier PRIDE: PXD039830. The deposited data are publicly available as of the date of publication. This paper also analyzes existing, publicly available data from ENCODE. Accession numbers are listed in the key resources table.
- This paper does not report original code.
- Any additional information required to reanalyze the data reported in this paper is available from the lead contact upon request.

EXPERIMENTAL MODEL AND STUDY PARTICIPANT DETAILS

Animals

Animal experiments were approved by the Institutional Animal Care and Use Committee at Massachusetts General Hospital (MGH) and were carried out in accordance with the Guide for Care and Use of Laboratory Animals (National Institutes of Health, Bethesda, MD). Mice were housed in a temperature and humidity-controlled barrier facility on a 12-hour light-dark schedule and fed *ad libitum* with standard rodent chow (Prolab RMH 3000; LabDiet, 380 ppm iron) until otherwise specified.

For RNA-Sequencing and proteomic studies, three-week-old wild-type 129S6/SvEvTac male mice were fed a purified AIN-93G iron-sufficient rodent diet formulated to contain 37 ppm iron as ferric citrate (Research Diets D08090806) or a matched, purified, high-iron diet containing 10,000 ppm carbonyl iron (Research Diets D08090805) for 4 weeks.

For experiments using c-Jun N-terminal kinase (JNK) inhibitor SP600125, four-week-old wild-type C57BL/6N (Taconic Farms) female mice were fed a purified iron-sufficient diet (48 ppm iron, Envigo-Teklad TD.80394) for 3 days. On day 4, half of the mice were switched to a matched, purified, high-iron diet (20,000 ppm iron, Envigo-Teklad TD.08496), while the remaining mice continued the iron-sufficient diet. Starting on day 3, mice in both groups received daily intraperitoneal injections of broad-spectrum JNK inhibitor SP600125 (2 mg/mouse, Tocris 1496/50), which blocks c-Jun phosphorylation, or DMSO for 5 days and were harvested 6 hours after the final injection.

To generate mice with deletion of *Jun* in endothelial cells, C57BL/6 mice harboring LoxP-flanked alleles of *Jun*[30] (provided by Richard Libby, Rochester, NY, USA) were bred to C57BL/6 mice expressing *Cre* recombinase under the control of an endothelial cell-specific Stabilin-2 (Stab2) promoter[31] (provided by Cyrill Géraud, Mannheim, Germany) to produce $Jun^{fl/fl}$;*Stab2-Cre*+ and $Jun^{fl/fl}$;*Stab2-Cre*- littermate controls. Six-week-old male and female mice were fed a purified iron-sufficient diet (48 ppm iron, Envigo-Teklad TD.80394) or a matched, purified, high-iron diet (10,000 ppm iron, Envigo-Teklad TD.08043) for 2 weeks. For Nrf-2 activator studies, $Jun^{fl/fl}$;*Stab2-Cre*+ and littermate *Cre*- mice were treated with 30 mmol/kg Nrf-2 activator CDDO-Im or solvent control by oral gavage for 6 hours.

For both manufacturers, matched, purified diets are identical with the exception of the amount and source of iron. According to the manufacturers, carbonyl iron is used for high-iron diets to avoid toxic effects of the iron salts at high concentrations and because it provides more elemental iron per gram. Ferric citrate is used in control diets because it is less complicated to incorporate and cheaper per unit iron. Iron-deficient diets are formulated without adding iron.

Cell culture

CD1 mouse primary liver sinusoidal endothelial cells (Cell Biologics CD-1017) were maintained in complete mouse endothelial cell medium with growth factor supplement following manufacturer's instructions (Cell Biologics M1168PF). The cells were used at passage 3 to 10 and maintained at 37°C in a 5% CO_2 95% air atmosphere. Although the cells are marketed as liver sinusoidal endothelial cells, since they were isolated using pan-endothelial marker CD31, we cannot irrefutably confirm the cells are solely sinusoidal in nature. Thus, we refer to this cell culture model as liver endothelial cells. Information about the sex of the animals from which the cells are isolated is not provided by the company.

To induce cellular iron loading, cells were incubated with 0–200 μg/ml ferric ammonium citrate for 2–12 hours. For transcriptional inhibition, cells were treated with 2 μg/ml actinomycin D or DMSO in the presence of 0–200 μg/ml ferric ammonium citrate for 2–12 hours.

For gene knockdown experiments, cells were transfected with 40 nM non-targeting control siRNA (Invitrogen 4390846 or Dharmacon D-001206-13-05) or siRNA targeting *Jun* (Invitrogen s68564 or Dharmacon M-043776-01-0005) using Lipofectamine RNAiMAX (Invitrogen) per the manufacturer's instructions for 48 hours prior to iron treatment as described above or treatment with 100 nM Nrf-2 activator CDDO-Im for 6 hours. Gene knockdown was confirmed by qRT-PCR and immunoblotting.

METHOD DETAILS

Fluorescence-activated cell sorting (FACS)

Liver endothelial cells were sorted from 7-week-old mice by FACS as previously described[9,19] using the monoclonal antibodies listed in Table S3, and the gating strategy provided in Lim et al.[19] Cells were first gated using FSC/SSC characteristics, and doublets were sequentially excluded by comparing FSC and SSC height and area signals. Endothelial cells were identified as CD45-, CD31^{+}, lineage-, MHCII-, CD64-, CD146+. Lineage was defined as: CD3e, CD19, CD90.2, CD326, Ly6G, NK1.1. Cells were sorted on a FACSAria II (BD Biosciences) by the Harvard Stem Cell Institute-Center for Regenerative Medicine Flow Cytometry Core Facility at MGH.

Magnetic-activated cell sorting (MACS)

Whole liver was incubated in liver dissociation enzymes following the manufacturer's instructions (Miltenyi 130-105-807). Single-cell suspensions were prepared using fine scissors and filtration through 100- and 30-μm cell strainers. Endothelial cells and Kupffer cells were isolated by magnetic separation using Cd146 microbeads (Miltenyi 130-092-007) and F4/80 microbeads (Miltenyi 130-110-443), respectively, following the manufacturer's instructions.

RNA-sequencing

RNA-sequencing was performed at the MGH NextGen Sequencing Core. Total RNA from FACS-sorted endothelial cells was isolated using PicoPure RNA Isolation Kit (Applied Biosystems) and RNA quality and concentration were assessed by using Agilent 2100 Bioanalyzer. Seventy ng total RNA was used for library construction using a Clontech SMARTer Ultra Low Input Kit. RNA sequencing was performed using Illumina HiSeq2000 Sequencing in High-Output mode, which offers 150–200 million reads per lane.

Quantitative proteomics

Quantitative mass spectrometry-based proteomics were performed as previously described.[51] Cells were homogenized by 20 passes through a 21-gauge (1.25 in. long) needle in lysis buffer (8 M Urea, 200 mM HEPES pH 8.5, 1x Roche protease inhibitors, 1x Roche PhosphoStop phosphatase inhibitors) at a protein concentration of ~5 mg/mL. The homogenate was sedimented by centrifugation at 20,000 x g for 5 min at 4°C. Proteins were subjected to disulfide bond reduction with 5 mM dithiothreitol (37°C, 25 min) and alkylation with 10 mM iodoacetamide (room temperature, 30 min in the dark). Excess iodoacetamide was quenched with 15 mM dithiothreitol (room temperature, 15 min in the dark).

Chloroform–methanol precipitation of proteins from cells was performed prior to protease digestion. In brief, four parts neat methanol was added to each sample and vortexed, one part chloroform was added to the sample and vortexed, and three parts water was added to the sample and vortexed. The sample was centrifuged at 10,000 rpm for 2 min at room temperature and washed twice with 100% methanol. Samples were resuspended in 200 mM HEPES pH 8.5 for digestion. Protein concentrations were determined by bicinchoninic acid assay.

For each of the samples, protein was digested at 37°C for 3 h with LysC protease at a 1:100 protease-to-protein ratio. Trypsin was then added at a 1:100 protease-to-protein ratio and incubated overnight at 37°C. TMT reagents were dissolved in anhydrous acetonitrile and added to the peptides in 200 mM HEPES, pH 8.5 and 30% v/v of acetonitrile at a 1:2 ratio. Following incubation at room temperature for 1 h, the reaction was quenched with hydroxylamine to a final concentration of 0.3% v/v. The TMT-labeled samples were combined at a 1:1 across all samples.

We fractionated the pooled TMT-labeled peptide sample using a High pH Reversed-Phase Peptide Fractionation Kit (Pierce 84868) per the manufacturer's instructions except the acetonitrile percentage used in the elution buffers and the concatenation strategy. Twelve fractions were collected using 7.5%, 10%, 12.5%, 15%, 17.5%, 20%, 22.5%, 25%, 27.5%, 30%, 35%, and 60% acetonitrile in 0.1% triethylamine (TEA). The samples were concatenated into six by combining as follows: 7.5% and 22.5%, 10% and 25%, 12.5% and 27.5%, 15% and 30%, 17.5% and 35%, 20% and 60%. Combined fractions were vacuum centrifuged to near dryness. Each fraction was desalted via StageTip, dried via vacuum centrifugation, and reconstituted in 5% acetonitrile, 5% formic acid for LC-MS/MS data acquisition.

Mass spectrometry data were collected using an Orbitrap Fusion and Fusion Lumos mass spectrometer (ThermoFisher) each coupled to a Proxeon EASY-nLC 1000 liquid chromatography pump (ThermoFisher). Peptides were separated on a 100 μm inner diameter microcapillary column packed with ~35 cm of Accucore150 resin (2.6 μm, 150 Å, ThermoFisher). We loaded ~1 μg of peptide onto the column for each sample injection.

Each analysis used the multi-notch MS3-based TMT method.[52] Each fraction was analyzed on both instruments resulting in a total of 12 RAW files. Using the Orbitrap Fusion, peptides were separated using a 150 min gradient of 3–24% acetonitrile in 0.125% formic acid at a flow rate of ~500 nL/min. The scan sequence began with an MS1 spectrum (Orbitrap analysis; resolution 120,000; mass range 350–1400 m/z; automatic gain control (AGC) target 5.0E5; maximum injection time 100 ms). Precursors for MS2/MS3 analysis were selected using a Top10 method and then selected for MS2/MS3 analysis.[53] MS2 analysis consisted of collision-induced dissociation (quadrupole ion trap analysis with turbo scan rate; AGC 2E4; normalized collision energy (NCE) 35; maximum injection time 150 ms). MS3 precursors were fragmented by high energy collision-induced dissociation (HCD) and analyzed using the Orbitrap (NCE 65; AGC 2E5; maximum injection time 150 ms, resolution was 50,000). Using the Orbitrap Fusion Lumos, peptides were separated using a 180 min gradient of 3–24% acetonitrile in 0.125% formic acid at a flow rate of ~500 nL/min. The scan sequence began with an MS1 spectrum (Orbitrap analysis; resolution 120,000; mass range 350–1400 m/z; AGC target 5.0E5; maximum injection time 120 ms). Precursors for MS2/MS3 analysis were selected using a Top10 method and then selected for MS2/MS3 analysis.[53] MS2 analysis consisted of collision-induced dissociation (quadrupole ion trap

analysis with turbo scan rate; AGC 2E4; NCE 35; maximum injection time 150ms). MS3 precursors were fragmented by HCD and analyzed using the Orbitrap (NCE 65; AGC 2.5E5; maximum injection time 150 ms, resolution was 50,000).

Mass spectra were processed using a Sequest-based in-house software pipeline.[52] Spectra were converted to mzXML using a modified version of ReAdW.exe. Database searching included all entries from the Mus musculus UniProt database. The database was concatenated with one composed of all protein sequences in the reversed order. Searches were performed using a 50-ppm precursor ion tolerance and a 1 Da product ion tolerance. These wide mass tolerance windows were chosen to maximize sensitivity in conjunction with Comet searches and linear discriminant analysis (LDA).[54,55] TMT tags on lysine residues and peptide N-termini (+229.163Da) and carbamidomethylation of cysteine residues (+57.021 Da) were set as static modifications, while oxidation of methionine residues (+15.995 Da) was set as variable. Peptide-spectrum matches (PSMs) were adjusted to a 1% false discovery rate (FDR).[56,57] PSM filtering was performed using LDA[55] and assembled further to a protein-level FDR of 1% across the entire dataset.[57] Proteins were quantified by summing reporter ion counts across all PSMs.[58] Reporter ion intensities were adjusted to correct for the isotopic impurities of the different TMT reagents according to manufacturer specifications. The signal-to-noise measurements of peptides assigned to each protein were summed and normalized such that the sum of the signal for all proteins in each channel was equivalent to account for equal protein loading. Finally, each abundance measurement was scaled, such that the summed signal-to-noise for that protein across all channels equaled 100, generating a relative abundance measurement.

Gene set enrichment analysis

Gene set enrichment analysis (GSEA Desktop v2.2) was performed on RNA-sequencing and proteomic datasets, excluding one-peptide detections and peptides without direct protein references. Gene sets (from MSigDB geneset c3.tft.v5.2) from RNA-sequencing and proteomic analyses were overlaid to identify repeating patterns and reverse effects in the proteomic group against transcription factor binding motif gene sets. We used a predefined, arbitrary threshold of 1.5 for Normalized Enrichment Score for both proteomics and RNA-seq analysis to shortlist transcription factors for further analysis. For overlap analysis, $p < 0.05$ was used to determine significant hits.

Gene expression by quantitative reverse-transcriptase polymerase chain reaction (qRT-PCR)

Total RNA was isolated from FACS-sorted endothelial cells using PicoPure RNA Isolation Kit (Applied Biosystems). RNA quality and concentration were assessed by using Agilent 2100 Bioanalyzer. First-strand cDNA was synthesized from 2.5 ng RNA using the SuperScript VILO cDNA Synthesis Kit (Invitrogen).

Total RNA was isolated from primary endothelial cell cultures, MACS-sorted cells, and frozen mouse tissues using RNeasy Mini or Micro Kit (Qiagen), or Pure-Link RNA Mini Kit (Invitrogen). First-strand cDNA was synthesized from 0.4 μg (MACS-sorted cells), 1 μg (mouse tissue) or 2 μg (endothelial cell cultures) of RNA by using the High-Capacity RNA-to-cDNA Kit (Applied Biosystems).

PCR reactions were performed using the PowerUp SYBR Green Master Mix (Applied Biosystems) on the QuantStudio3 Real-Time PCR system (Applied Biosystems) and analyzed using QuantStudio3 Design and Analysis Software (v.1.5.1). Gene-specific primers are listed in Table S4.

Western blotting

Cells were homogenized in RIPA lysis buffer with protease and phosphatase inhibitors and protein concentration was measured by DC-protein assay (Bio-Rad). Proteins were separated by SDS-PAGE on NuPAGE 4–12% Bis-Tris protein gels (Invitrogen) and transferred to nitrocellulose membranes, which were blocked in 5% w/v dried nonfat milk or bovine serum albumin in TBS with 0.05% Tween 20 and incubated with the primary antibodies listed in Table S3 in blocking buffer overnight at 4°C. Protein blots were visualized by chemiluminescence using the GeneSys G:Box Mini 6 imaging system (Syngene v1.6.1.0). See Figure S7 for uncropped Western blot images.

Chromatin immunoprecipitation (ChIP) qRT-PCR

Frozen liver pieces from mice fed iron-deficient (2–6 ppm iron, Envigo-Teklad TD.80396) or iron-sufficient (48 ppm iron, Envigo-Teklad) diets were fixed in 1% formaldehyde to crosslink DNA-protein complexes. Fixed liver pieces were incubated in cell lysis buffer with added protease inhibitors (Roche) and manually disrupted by Dounce homogenization. Nuclei were collected by centrifugation at 2,000 x g for 5 min, incubated in nuclear lysis buffer, and sonicated using Qsonica 800R to shear chromatin. Supernatant was subjected to immunoprecipitation overnight at 4°C with continuous rotation using 1–4 μg of antibody listed in Table S3. Normal IgG was used as a negative control to control for nonspecific binding, and histone antibody H3K4me3 as a positive control. Following overnight incubation, samples were incubated with precleared protein A/G beads (Millipore 16–663) for 2 hours. Chromatin was eluted by heating to 65°C for 15 min and crosslinks reversed by heating to 65°C for 12–16 hours. Chromatin was treated with RNAse A for 1 hour at 37°C followed by incubation with proteinase K for 2 hours at 45°C and purified using QIAquick PCR purification kit (Qiagen). Eluted DNA was subjected to qRT-PCR using the primers listed in Table S4. Data were normalized by fold enrichment relative to the IgG control.

ChIP-sequencing analysis

ChIP-sequencing data from human umbilical vein endothelial cells for the *BMP6* locus were available from ENCODE.[21] Datasets were downloaded from the ENCODE portal[20] using the following accession numbers: ENCSR000ALG, ENCSR578QSO, ENCSR000ALB, ENCSR000EFA,

and ENCSR000EOQ. Sequences were aligned to the GRCh38 genome (Genome Reference Consortium) and visualized using the UCSC genome browser (http://genome.ucsc.edu).[59–61]

Nonheme iron measurements

Serum nonheme iron and unsaturated iron binding capacity were measured by colorimetric assay (Pointe Scientific) to calculate transferrin saturation per the manufacturer's instructions. For tissue nonheme iron concentrations (in μg/g wet tissue weight), tissue pieces were digested in acid solution (10% w/v trichloroacetic acid, 25.8% v/v hydrochloric acid) at 65°C for 20 hours, and supernatant was analyzed by colorimetric assay using chromogen reagent (1% w/v bathophenanthroline sulfonate 1% v/v thioglycolic acid, in 5 volumes saturated sodium acetate and 5 volumes water) and an iron standard (1000-ppm iron).[62]

Complete blood counts

Complete blood counts were measured on whole blood collected in K_2-EDTA coated microtainer tubes (Beckton Dickinson) at the MGH Center for Comparative Medicine Clinical Pathology Laboratory.

Perl's iron stain and TUNEL stain

Perl's iron stain was performed on paraformaldehyde-fixed liver endothelial cell cultures using Iron Stain Kit (American MasterTech KTIRO) and enhanced using 3,3′-Diaminobenzidin (Vector Labs SG). TUNEL stain was performed on paraformaldehyde-fixed liver endothelial cell cultures using fluorescence TUNEL assay kit following the manufacturer's instructions (Cell Signaling 25879). Images were acquired using a Keyence BZ-X710 microscope.

QUANTIFICATION AND STATISTICAL ANALYSIS

Statistical analysis was performed using Prism 9 (GraphPad). Data are presented as individual values with bars representing the mean ± SEM unless otherwise specified. Shapiro-Wilk test was used to test normality. For comparisons between two groups, two-tailed Student's *t* test was used for normally distributed values or Mann–Whitney *U* test for non-normally distributed values. For comparisons among more than two groups, statistical differences were determined by one-way ANOVA with Holm-Sidak multiple comparisons test for normally distributed values or Kruskall-Wallis test with Dunn's method of multiple comparisons for non-normally distributed values. A p value of less than 0.05 was considered significant.